



# Preparation of Fe/C-MgCO<sub>3</sub> micro-electrolysis fillers and mechanism of phosphorus removal

Yanhe Han<sup>1</sup> · Zhimin Su<sup>1</sup> · Xuejiao Ma<sup>1</sup> · Xiaolu Fu<sup>1</sup> · Han Xu<sup>1</sup> · Lina Liu<sup>1</sup> · Meili Liu<sup>1</sup>

Received: 16 February 2022 / Accepted: 13 September 2022 / Published online: 21 September 2022  
© The Author(s), under exclusive licence to Springer-Verlag GmbH Germany, part of Springer Nature 2022

## Abstract

Iron-carbon micro-electrolysis is effective for the removal of phosphorus in wastewater; however, meeting the stringent emission standards required for treatment is difficult. To meet these treatment standards, modified micro-electrolytic fillers were prepared from iron dust, powdered activated carbon, clay, and additives using an elevated temperature roasting process under an inert atmosphere. The results show that among several additives, the modified micro-electrolytic (Fe/C-MgCO<sub>3</sub>) fillers using MgCO<sub>3</sub> were the most effective at phosphorus removal. The preparation conditions for the Fe/C-MgCO<sub>3</sub> fillers and their effects on phosphorus removal performance were investigated. Under the optimal preparation conditions (calcination temperature: 800 °C, Fe/C = 4:1, clay content 20%, and 5% MgCO<sub>3</sub>), the filler yielded a high compressive strength of 3.5 MPa, 1 h water absorption rate of 25.7%, and specific surface area and apparent density of 154.2 m<sup>2</sup>/g and 2689.2 kg/m<sup>3</sup>, respectively. The iron-carbon micro-electrolysis process removed 97% of phosphorus in the wastewater by using the Fe/C-MgCO<sub>3</sub> fillers, which was 14% more than the Fe/C filler. Electrostatic adsorption and surface precipitation were identified as the main phosphorus removal mechanisms, and the surface of the Fe/C-MgCO<sub>3</sub> filler was continuously updated. These results demonstrated that Fe/C-MgCO<sub>3</sub> is a promising filler for phosphorus removal in water treatment.

**Keywords** Iron-carbon micro-electrolysis · Phosphorus · Modified micro-electrolytic filler · Magnesium metal oxides · Wastewater · Mechanism

## Introduction

The significant increase in water consumption following the improvement of the living standards of the rural residents in China has resulted in the generation of large quantities of rural sewage (Bi and Guo 2020). The obsolete rural sewage treatment technology and facilities and low sewage treatment rate, have resulted in a sizable proportion of untreated wastewater being directly disposed of into the environment, thereby causing considerable phosphorus leakage to the environment. Excess phosphorus in water bodies causes ecological damage and leads to eutrophication (Zou and Wang 2016). The inhibition of exogenous phosphorus discharging

into water bodies is a potential solution to this problem and a relatively sustainable management strategy (Kong et al. 2019).

At present, chemical (Yang et al. 2010), biological (Park et al. 2009), and iron-carbon methods are the commonly used techniques for phosphorus removal. Chemical phosphorus removal entails the addition of metal salts (such as aluminum, iron, calcium, and magnesium) to phosphorus-containing wastewater; these elements react with phosphate to form precipitates that separate from the water (Guo et al. 2014). Chemical methods have been widely used for phosphate removal. However, owing to the extensive consumption of chemicals and difficulties in treating chemical sludge, biological methods have been strongly promoted and applied (Barat et al. 2011; Tang et al. 2012). Biological phosphorus removal entails the use of polyphosphate-accumulating organisms to remove phosphate from wastewater (Ramasahayam et al. 2014) and convert it into sludge in the form of intracellular polyphosphate. Biological methods have been extensively applied in the removal of phosphorus from wastewater because

Responsible Editor: Angeles Blanco

✉ Yanhe Han  
hanyanhe@126.com; hanyanhe@bipt.edu.cn

<sup>1</sup> Department of Environmental Engineering, Beijing Institute of Petrochemical Technology, Beijing 102617, People's Republic of China

they are remarkably economical and non-toxic. However, these biological methods barely meet the requirements of the increasingly stringent laws (Ren et al. 2020). In contrast, iron-carbon methods have the advantages of simple operation, low cost, and environmental friendliness, and are considered promising technologies for phosphorus removal.

The iron-carbon method is also referred to as iron-carbon micro-electrolysis (IC-ME), and is used for phosphorus removal from wastewater; this method is based on electrochemistry, redox, adsorption, and flocculation (Zhao et al. 2020). Recently, IC-ME has been widely used in phosphorus wastewater treatment. Zhou et al. (Zhou et al. 2014) applied IC-ME technology to degrade and remove phosphates from discharged circulating cooling water, and indicated that the technique was effective for phosphorus removal. During the IC-ME process, a nascent iron floc was generated, which may contribute to phosphorus precipitation in wastewater (Zhu et al. 2014). A phosphorus removal rate of 88% was achieved under optimized reaction conditions using the orthogonal tests of the IC-ME system. However, the traditional IC-ME process fails to meet the specified emission standards, especially when hardening occurs during long-term operation (Zhang et al. 2018).

The filler in the IC-ME system, which affects the number of active sites and mass transfer efficiency, plays a key role in the removal of phosphorus. The pollutant removal performance of binary IC-ME fillers can be significantly improved by compositing with metal (Li et al. 2021b). Li et al. (Li et al. 2017) have noted that solid metal oxides such as magnesium oxide and calcium oxide can be used as kinks for metal sources. Magnesium oxide and calcium oxide are inexpensive, non-toxic alkaline earth metal oxides with a strong affinity for phosphates, and have been widely used as active components for the removal of phosphorus (Liu et al. 2021b). Therefore, loading magnesium oxide or calcium oxide onto carriers can improve the efficacy of phosphorus removal (Zhu and Xing 2018). Phosphorus removal in IC-ME can be hypothesized to be effectively improved by the application of magnesium oxide or calcium oxide to the iron-carbon fillers. However, studies on the composition of magnesium oxide or calcium oxide composited iron-carbon fillers used for phosphorus removal are very limited.

The specific objectives of this study were to prepare magnesium oxide or calcium oxide–modified Fe/C fillers and explore and identify the modified fillers with optimal phosphorus removal performance. The preparation parameters were optimized for the modified filler and the treatment efficiency of phosphorus wastewater was determined when the modified fillers worked for a long period. Scanning electron microscopy (SEM), energy-dispersive spectroscopy (EDS), X-ray photoelectron spectroscopy (XPS), and X-ray diffraction (XRD) were used to explore the phosphorus removal mechanism

and provide a theoretical basis for the practical application of modified fillers.

## Materials and methods

### Materials

Iron powder, activated carbon powder, additives (MgO, MgCO<sub>3</sub>, CaMg(CO<sub>3</sub>)<sub>2</sub>, and CaCO<sub>3</sub>), ammonium bicarbonate, and sodium silicate were obtained from Shanghai Macklin Biochemical Technology Co., Ltd. (Shanghai, China). Dolomite powder and clay were obtained from Stone Factory (Hebei, China).

Experimental influent water was artificially prepared to simulate rural domestic sewage. C<sub>6</sub>H<sub>12</sub>O<sub>6</sub>, NH<sub>4</sub>Cl, and K<sub>2</sub>HPO<sub>4</sub> were used as the sources of carbon, nitrogen, and phosphorus, respectively. The pH was adjusted using a 5% HCl or 5% NaOH solution. The characteristic values of the artificial simulated wastewater are listed in Table 1. All the chemical solutions were prepared using deionized water in the experiments.

### Modified micro-electrolytic filler preparation

Modified fillers were prepared with iron powder, activated carbon powder, and clay as the basic raw materials; Na<sub>2</sub>SiO<sub>3</sub> as the binder; NH<sub>4</sub>HCO<sub>3</sub> as a pore-forming agent; and MgCO<sub>3</sub>, MgO, CaCO<sub>3</sub>, and dolomite powder as the additives. The composition of the fillers prepared in this study is listed in Table 2.

The preparation process of the modified micro-electrolysis filler included the following steps: first, the reduced iron powder, activated carbon powder, clay, pore-forming agent, and additives were uniformly mixed in the mass percentages of 31.5:31.5:30:4:3. A slurry of suitable viscosity was formed by adding 12% distilled water and 7% binder to the mixture. The mixture was formed into spheres with a diameter of 8–12 mm using a pelletizer. The prepared wet fillers were dried at 105 °C in an air oven for 2 h before being placed in a tube furnace and maintained at 800 °C for 1 h under a nitrogen atmosphere; subsequently, the fillers were cooled to room temperature.

After cooling in a furnace, the micro-electrolytic fillers comprising different additives, MgO, MgCO<sub>3</sub>, CaCO<sub>3</sub>, and CaMg(CO<sub>3</sub>)<sub>2</sub>, were produced and named Fe/C-MgCO<sub>3</sub>, Fe/C-MgO, Fe/C-CaCO<sub>3</sub>, and Fe/C-CaMg(CO<sub>3</sub>)<sub>2</sub>, respectively.

**Table 1** Simulated wastewater composition

Composition	COD (mg/L)	NH <sub>4</sub> <sup>+</sup> -N (mg/L)	TP (mg/L)	pH
Content	300	40	5–7	6.5–7.5

**Table 2** Composition of filler samples

Material	Iron powder (wt%)	Powdered activated carbon (wt%)	Clay (wt%)	Na <sub>2</sub> SiO <sub>3</sub> (wt%)	NH <sub>4</sub> HCO <sub>3</sub> (wt%)	Additive (wt%)
Content	30–60	10–40	10–50	3	0.5	0–15

## Reactor and operation procedure

**Instruments and procedure** The experimental apparatus comprising micro-electrolytic fillers and a sequencing batch reactors system are illustrated in Fig. 1. The air was supplied by an air pump, and the gas flow rate was maintained in the range of 0.18–0.2 m<sup>3</sup>·h<sup>-1</sup>. Gas was supplied at the bottom of the reactor through an aerator. Water pumps were used to deliver the untreated wastewater. The residence time of water in each column was 120 min. The filler mass was 50 g, and the reaction volume of the simulated wastewater solution was 100 mL in each column. The initial pH of 3 was adjusted with 5% HCl.

Samples were obtained at various times (0, 10, 30, 60, 90, 120, 180, and 240 min) and filtered to determine the total phosphorus (TP) content. The pH of the water sample was adjusted to 8.5 via the dropwise addition of 5% NaOH or 5% HCl.

The effects of the type of additive (MgO, MgCO<sub>3</sub>, CaCO<sub>3</sub>, and CaMg(CO<sub>3</sub>)<sub>2</sub>), calcination temperature (600, 700, 800, 900, and 1000 °C), Fe/C ratio (1:1, 2:1, 4:1, 6:1, and 8:1), clay content (10%, 20%, 30%, 40%, and 50%), and additive content (0%, 1%, 3%, 5%, 10%, and 15%) on TP removal were investigated. Finally, the optimum preparation conditions for the modified filler were determined.

## Analytical methods

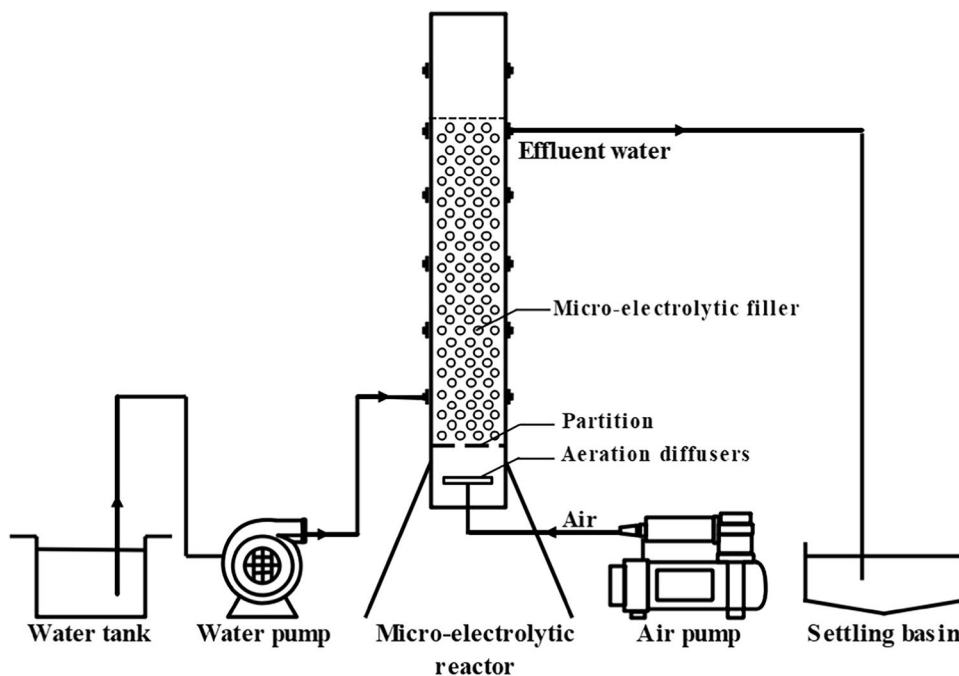
The pH of the solution was determined using a portable pH meter (PHSJ-3F, Shanghai Instrument & Electrical Scientific Instrument Co., Ltd., China). TP was determined using ammonium molybdate spectrophotometry (5B-1(V8), Lianhua Science & Technology, China). The surface morphologies of the packing surfaces were observed using SEM and EDS (SEM-EDS; SSX-550, Shimadzu, Japan). Brunauer–Emmett–Teller (BET) (Micromeritics ASAP 2460, China) was used to measure the specific surface area of the filler. XPS (ESCALAB 250Xi, Thermo Fisher Scientific, USA) was used to determine the composition of the filler surface after the reaction. XRD (PANalytical X-ray Diffractometer Model X PerT3, Netherlands) was used to scan the filler before and after the reaction.

The removal rate of TP can be calculated as follows (Eq. 1):

$$D(\%) = (C_0 - C) / C_0 \times 100 \quad (1)$$

where  $C_0$  and  $C$  are the initial and residual concentrations of TP, respectively.

**Fig. 1** Schematic of experimental apparatus for iron-carbon micro-electrolysis



## Results and discussion

### Characterization of modified micro-electrolytic filler

The morphology of the filler surface has an important influence on the heterogeneous reaction because the reaction is performed mainly at the interface (Li et al. 2018). Therefore, the surface morphology of the modified micro-electrolytic filler was investigated. The SEM images of the surfaces of the fillers, comprising different additives and sintered at 800 °C under an N<sub>2</sub> atmosphere, are shown in Fig. 2.

Significantly, compared with the relatively loose microstructures of Fe/C (Fig. 2a) and Fe/C-MgCO<sub>3</sub> fillers (Fig. 2b), those of Fe/C-CaCO<sub>3</sub> (Fig. 2c), Fe/C-MgO (Fig. 2d), and Fe/C-CaMg(CO<sub>3</sub>)<sub>2</sub> (Fig. 2e) were denser. This difference could be attributed to the different chemical properties of the additives. Gas is not generated in the preparation process because the decomposition temperature of calcium oxide and dolomite exceeds 800 °C. This hypothesis was confirmed by the XRD patterns of the five fillers (Fig. 3). Therefore, a large porous structure was not formed inside the Fe/C filler, which was not conducive to phosphorus removal (Li et al. 2021a; Wang et al. 2014) (Fig. 2c and e). Magnesium oxide powder can also block the pores of the Fe/C fillers, thereby reducing the porous structure (Fig. 2d).

Decomposed MgCO<sub>3</sub> can produce CO<sub>2</sub> gas at 800 °C, resulting in a porous structure in the Fe/C-MgCO<sub>3</sub> filler (Liu et al. 2011) (Fig. 2b). The significant number of pores

in Fe/C-MgCO<sub>3</sub> (Fig. 2b) could potentially produce an increased water absorption, and phosphorus removal rate (Sawada et al. 1979).

To further study the microporous structure of the fillers, the adsorption and desorption isotherms of N<sub>2</sub> at 77 K for Fe/C, Fe/C-MgCO<sub>3</sub>, Fe/C-MgO, Fe/C-CaCO<sub>3</sub>, and Fe/C-CaMg(CO<sub>3</sub>)<sub>2</sub> were investigated. The results are shown in the inset image of Fig. 4. A type IV sorption isotherm and an H1-type hysteresis loop were observed for each sample within a relative pressure range ( $P/P_0$ ) of 0.4–0.9 (Xie et al. 2018). An increase in N<sub>2</sub> adsorption was clearly observed in the hysteresis loop following the addition of MgCO<sub>3</sub>. These results indicate that macropores existed in the MgCO<sub>3</sub>-modified iron-carbon filler (Ponvel et al. 2010).

The pore size distribution of the five fillers in the range of 2–14 nm, as calculated from the nitrogen adsorption–desorption data, is illustrated in Fig. 4. The five fillers had obvious peaks in the range of 3–5 nm. The mesopore peak area of Fe/C-MgCO<sub>3</sub> was 1.2 times higher than that of Fe/C. This indicates that the Fe/C-MgCO<sub>3</sub> filler has more mesopores and macropores than the Fe/C packing, which may be due to the gas generated by the decomposition of MgCO<sub>3</sub> during the pyrolysis process (Kong et al. 2013; Liu et al. 2011).

The BET analysis results are shown in Table 3. Among all the prepared fillers, the Fe/C-MgCO<sub>3</sub> filler had the largest surface area and pore volume, which was also confirmed by SEM. This may facilitate phosphorus removal.

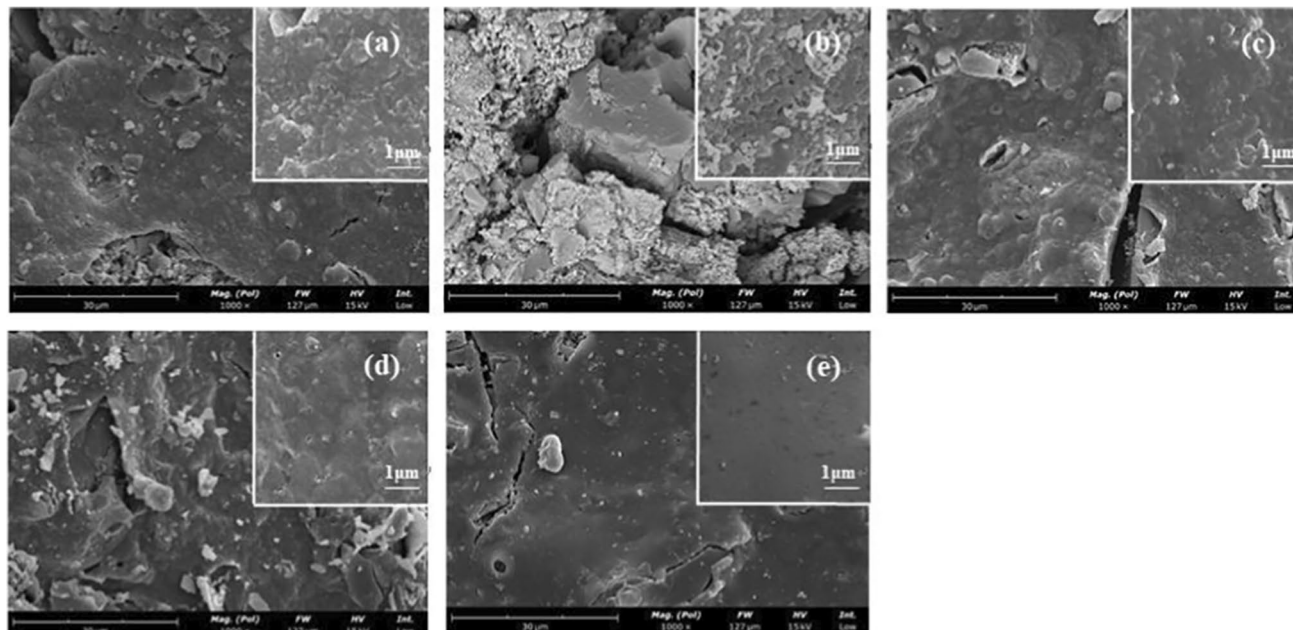


**Fig. 2** Scanning electron microscopy (SEM) images of the surfaces of the fillers: **a** Fe/C; **b** Fe/C-MgCO<sub>3</sub>; **c** Fe/C-CaCO<sub>3</sub>; **d** Fe/C-MgO; and **e** Fe/C-CaMg(CO<sub>3</sub>)<sub>2</sub>

**Fig. 3** Pore size distribution of packing (insert image: adsorption–desorption (AD) isotherms)

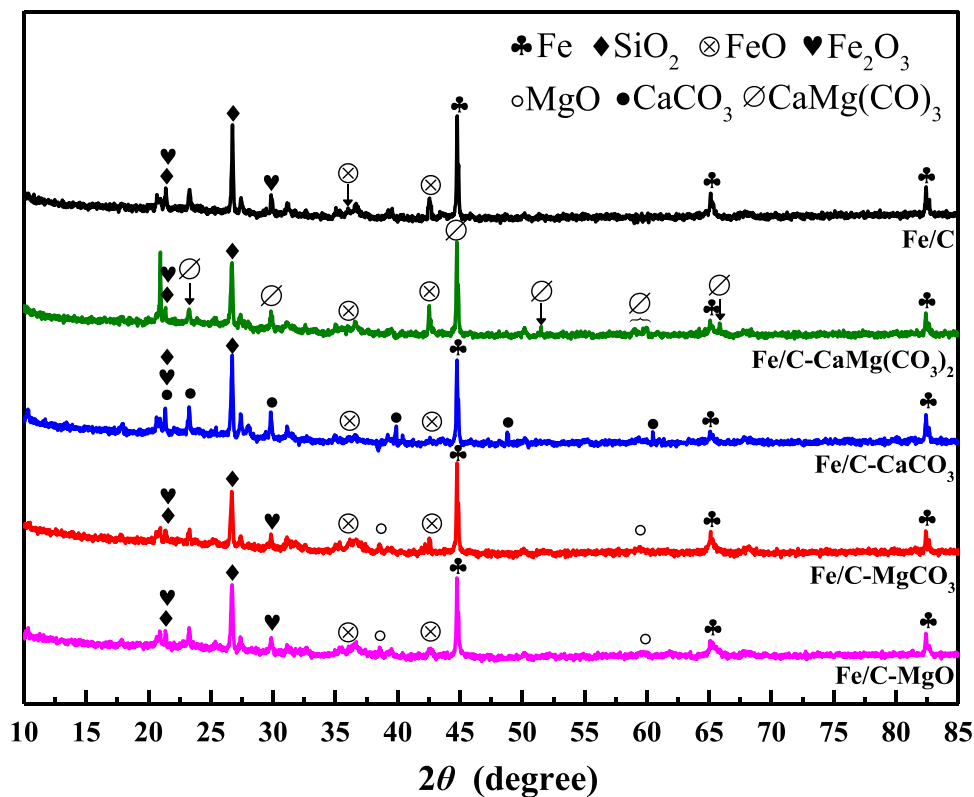
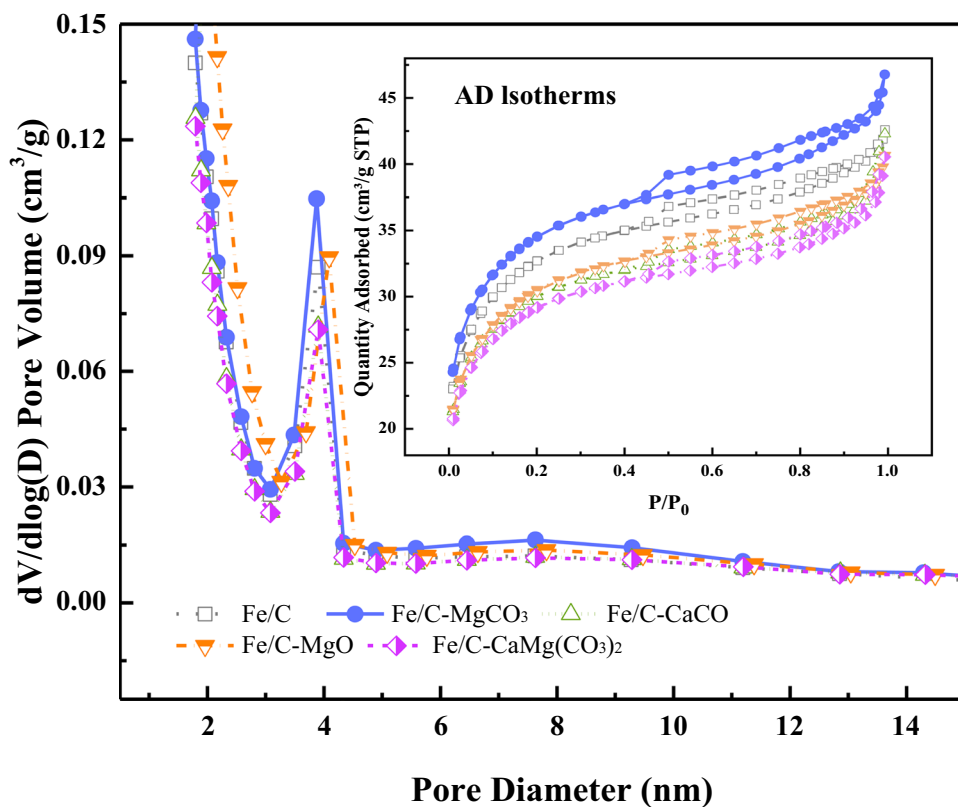


**Fig. 4** XRD patterns of five fillers





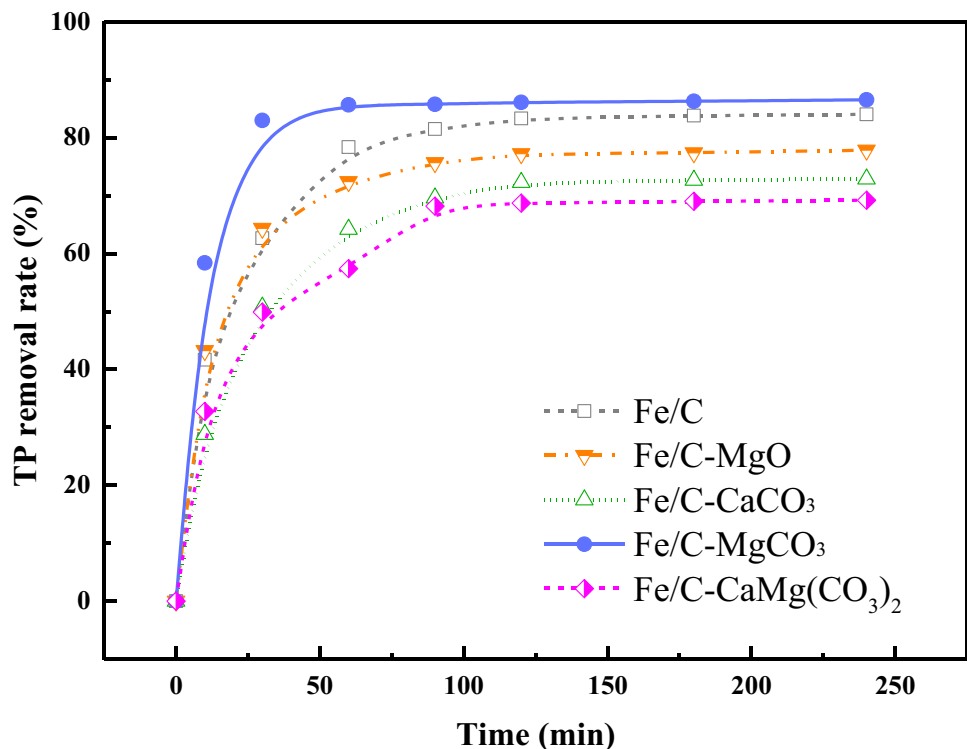
### TP removal performance of various additives

The TP removal rate of Fe/C, Fe/C-MgCO<sub>3</sub>, Fe/C-MgO, Fe/C-CaCO<sub>3</sub>, and Fe/C-CaMg(CO<sub>3</sub>)<sub>2</sub> is illustrated in Fig. 5. The capacity of the phosphorus removal of the Fe/C-MgCO<sub>3</sub> filler was higher than that of the other modified iron-carbon fillers. The capacities of the phosphorus removal decreased as follows: Fe/C-MgCO<sub>3</sub> > Fe/C > Fe/C-MgO > Fe/C-CaCO<sub>3</sub> > Fe/C-CaMg(CO<sub>3</sub>)<sub>2</sub>. The efficiency of the phosphorus removal by Fe/C-MgCO<sub>3</sub> was higher than that of Fe/C. These adsorption and desorption isotherm results indicate that the specific surface area and pore size of Fe/C-CaCO<sub>3</sub> are higher than those of Fe/C. A relatively large specific surface area and porosity facilitate contact between the phosphorus wastewater and fillers, which may increase the number of functional sites on the filler surface (Kang et al. 2019a), and could improve the efficiency of micro-electrolysis reactions.

**Table 3** Brunauer–Emmett–Teller (BET) analysis of packing

Sample	S <sub>BET</sub> (m <sup>2</sup> /g)	S <sub>micro</sub> (m <sup>2</sup> /g)	V <sub>total</sub> (m <sup>3</sup> /g)
Fe/C	119.19	57.86	0.07
Fe/C-MgCO <sub>3</sub>	125.97	61.62	0.07
Fe/C-MgO	111.09	52.60	0.06
Fe/C-CaCO <sub>3</sub>	109.49	54.58	0.07
Fe/C-CaMg(CO <sub>3</sub> ) <sub>2</sub>	106.48	53.36	0.06

**Fig. 5** Effects of type of additive on total phosphorus (TP) removal. Experimental conditions: calcination temperature = 800 °C, Fe/C ratio = 4:1, clay content = 30%, and additive content = 3%



In addition, the results of the experiment described in the “Characterization of modified micro-electrolytic filler” section indicated that the specific surface area of the other modified fillers was relatively small, and the number of active sites decreased significantly, thereby reducing the treatment efficacy on the phosphorus-contaminated wastewater. Therefore, MgCO<sub>3</sub> was selected as an additive for the modified micro-electrolytic filler in subsequent experiments to further investigate the optimization and reaction mechanism of phosphorus removal.

### Effect of single-factor on Fe/C-MgCO<sub>3</sub> filler optimization

#### Calcination temperature

The calcination temperature is a crucial factor in preparing micro-electrolytic fillers to determine their strength and effectiveness in wastewater treatment. Figure 6a illustrates the effect of the calcination temperature on the TP removal ability of the Fe/C-MgCO<sub>3</sub> filler during the micro-electrolysis reaction. The TP removal rate of the Fe/C-MgCO<sub>3</sub> filler gradually increased and then decreased as the calcination temperature increased. The highest TP removal rate (86.30%) was achieved when the calcination temperature was 800 °C, and the phosphorus removal effects of the Fe/C-MgCO<sub>3</sub> filler were reduced when the temperature was higher or lower than 800 °C.

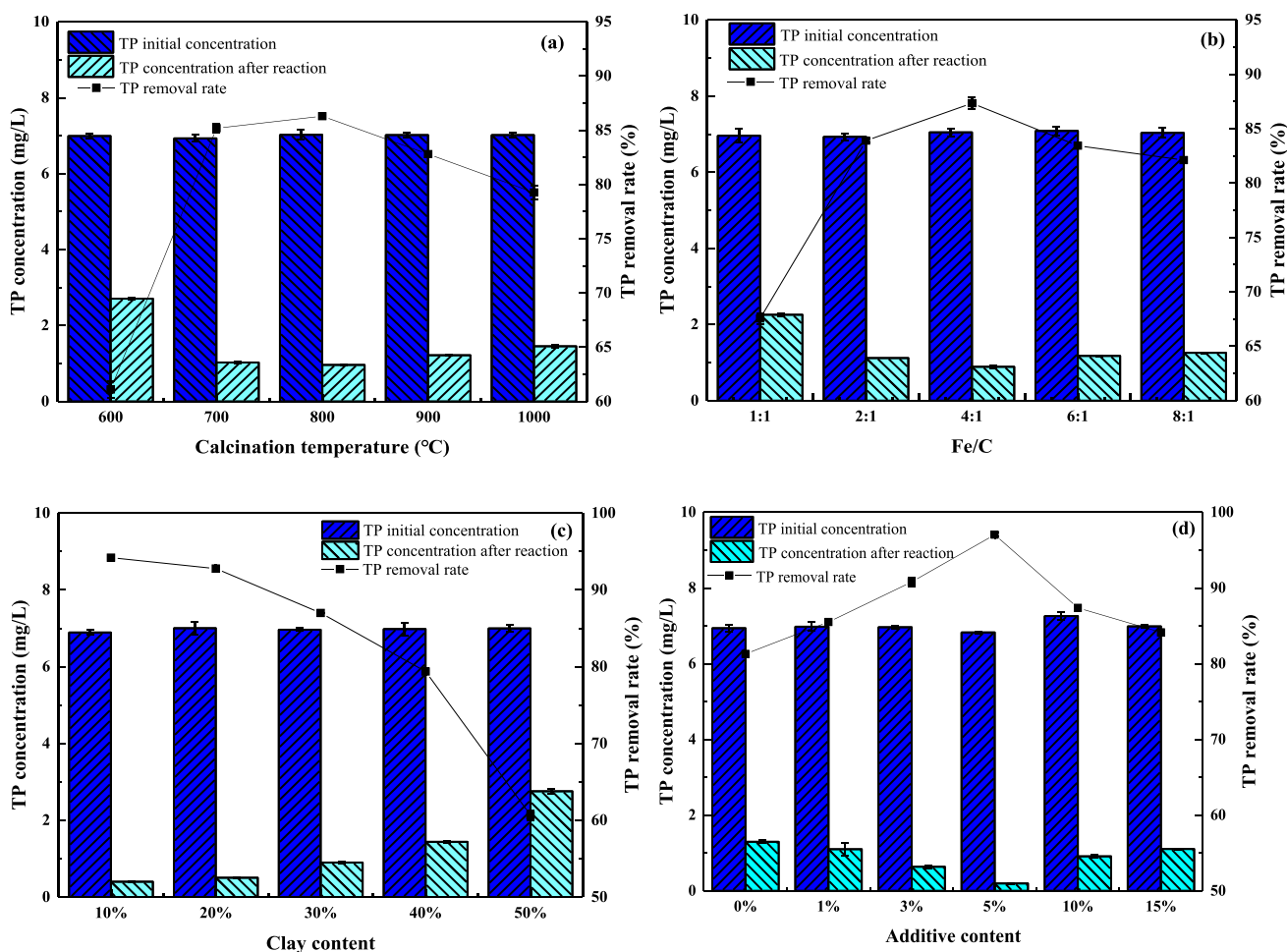


**Fig. 6** **a** Effect of calcination temperature on total phosphorus (TP) removal from wastewater at 120 min. Experimental conditions: Fe/C=4:1, clay content=30%, and additive content=3%. **b** Effect of Fe/C ratio on TP removal from phosphorus wastewater at 120 min. Experimental conditions: calcination temperature=800 °C, clay content=30%, and additive content=3%. **c** Effect of clay content on TP

removal of phosphorus wastewater at 120 min. Experimental conditions: calcination temperature=800 °C, Fe/C=4:1, and additive content=3%. **d** Effect of additive content on TP removal of phosphorus wastewater at 120 min. Experimental conditions: calcination temperature=800 °C, Fe/C=4:1, and clay content=20%

When the temperature was lower than 800 °C, the specific surface area and porosity of the filler were lower because the  $\text{MgCO}_3$  could not be decomposed, thereby impacting the phosphorus removal effect (Kang et al. 2019b). When the calcination temperature increased, the high-temperature decomposition of the  $\text{MgCO}_3$  in the modified micro-electrolytic filler increased the pore space of the filler and then increased the contact area between the filler and wastewater (Devasahayam and Strezov 2018). Hence, the treatment performance of the modified micro-electrolytic filler for phosphorus wastewater was gradually enhanced.

When the calcination temperature was greater than 800 °C, the clay in the filler melted and filled the spaces between the unfused particles, resulting in a decrease in the specific surface area and porosity (Mi et al. 2021). Fillers with lower specific surface areas and porosity are less

effective for phosphorus-containing wastewater treatment. Therefore, the selected calcination temperature of the subsequent filler preparation was 800 °C.

#### Fe/C ratio

In the IC-ME system, the number of primary batteries, which formed between iron and activated carbon (Liu et al. 2007), directly affects the treatment effect of the filler in the phosphorus wastewater. Therefore, the Fe/C ratio was investigated for its efficiency in TP removal from wastewater; the results are illustrated in Fig. 6b. The TP removal rates were 67.55%, 83.89%, 87.33%, 83.43%, and 82.12%, corresponding to the Fe/C mass ratios of 1:1, 2:1, 4:1, 6:1, and 8:1, respectively.

The efficiency of TP removal from wastewater reached a maximum at an Fe/C ratio of 4:1 (87.33%). This was because the molar volume ratio of Fe/C was close to 1:1 when the mass ratio of Fe/C was close to 4:1, which could result in the largest number of primary batteries formed between iron and activated carbon (Kang et al. 2019a). The adsorption of phosphorus was dominant under an excessively low Fe/C ratio because of the strong adsorption effect of carbon (Yang et al. 2021). Conversely, an excessively high Fe/C ratio resulted in a high filler abrasion rate and reduced number of primary batteries (Mi et al. 2021). Therefore, the treatment efficiency of the removal of phosphorus from wastewater was reduced. Hence, an Fe/C ratio of 4:1 was selected for the subsequent experiments.

### Clay content

Clay has excellent properties such as plasticity, binding, shrinkage, sintering, and refractoriness, and acts as a binder and skeleton in fillers (Riley 2006). However, clay is an inactive component of the filler that would inhibit phosphorus removal. The effect of the clay content on TP removal warrants investigation. The TP removal rate decreased as the clay content increased (Fig. 6c). The highest TP removal rate of 94% was achieved when the clay content in the fillers was 10%. This result was mainly attributed to the diminished phosphorus removal caused by the reduced iron and carbon contents in the IC-ME system, resulting from the increase in the clay content.

The low clay content complicated the formation of the fillers; thus, their compressive strength was insufficient. The compressive strengths of the fillers comprising different clay contents are compared in Table 4. When the clay content was 10%, the compressive strength did not meet the standard for fill use (Kang et al. 2019a). However, when the clay content was greater than 20%, the compressive strength fulfilled the standards for a filler. Therefore, a 20% clay content was determined to be suitable after considering the effectiveness

**Table 4** Clay contents and compressive strengths of modified fillers

Clay content (%)	10	20	30	40	50
Compressive strength (MPa)	1.75	3.50	4.33	5.09	5.99

**Table 5** Physical properties of modified Fe/C-MgCO<sub>3</sub> filler

Type	Specific surface area (m <sup>2</sup> /g)	Apparent density (kg/m <sup>3</sup> )	Bulk density (kg/m <sup>3</sup> )	Void fraction (%)	Coefficient of water absorption (%)	Compressive strength (MPa)	Grain size (mm)
Modified fillers	154.2	2689.2	694.4	74.9	25.7	3.5	9
Standard	≥ 0.5	–	≥ 600, < 700	≥ 40	–	–	< 19

of the phosphorus removal and compressive strength of the filler.

### Additive content

In the IC-ME system using Fe/C-MgCO<sub>3</sub> as a filler, MgCO<sub>3</sub> (as an additive in the filler) can react with PO<sub>4</sub><sup>3-</sup> in the wastewater to form a precipitation to provide an appropriate reaction surface. Figure 6d compares the effect of using different MgCO<sub>3</sub> contents (0%, 1%, 3%, 5%, 10%, and 15%) on the removal of TP.

The removal of TP increased sharply when the quantity of MgCO<sub>3</sub> increased from 0 to 5%, as illustrated by Fig. 6d. When the quantity of MgCO<sub>3</sub> was 5%, the removal rate of TP reached the maximum value of 97.0%. The rate of removal decreased when the quantity of MgCO<sub>3</sub> exceeded 5%. Hence, the addition of MgCO<sub>3</sub> improved the performance of the micro-electrolytic filler for the removal of phosphorus. However, when the MgCO<sub>3</sub> concentration was excessive, the treatment performance of the modified filler was inhibited. Therefore, 5% was selected as the optimum quantity of MgCO<sub>3</sub>.

### Performance of modified Fe/C-MgCO<sub>3</sub> filler

The bulk density, apparent density, water absorption, void fraction, specific surface area, compressive strength, and grain size were selected for the filler performance analysis, based on “Lightweight aggregates and its test methods” (China, GB/T17431.1–2010) and artificial ceramsite filter material for water treatment (China, CJ/T299-2008). The analysis factors and their results are listed in Table 5.

Compared with the standard, the Fe/C-MgCO<sub>3</sub> filler had a lower water adsorption rate (25.7%), higher compressive strength (3.5 MPa), higher specific surface area (154.2 m<sup>2</sup>/g), larger void fraction (74.9%), and lighter bulk density (694.4 kg/m<sup>3</sup>).

The elementary composition of the filler surface was studied via EDS (Fig. 7), and the mass percentages of various elements are presented in Fig. 7. The elemental analysis via EDS revealed that the surface of the filler consisted of carbon, oxygen, magnesium, aluminum, silicon, calcium, and iron atoms. Silicon and aluminum were part of the skeletal structure of the filler, and the metal ions such as



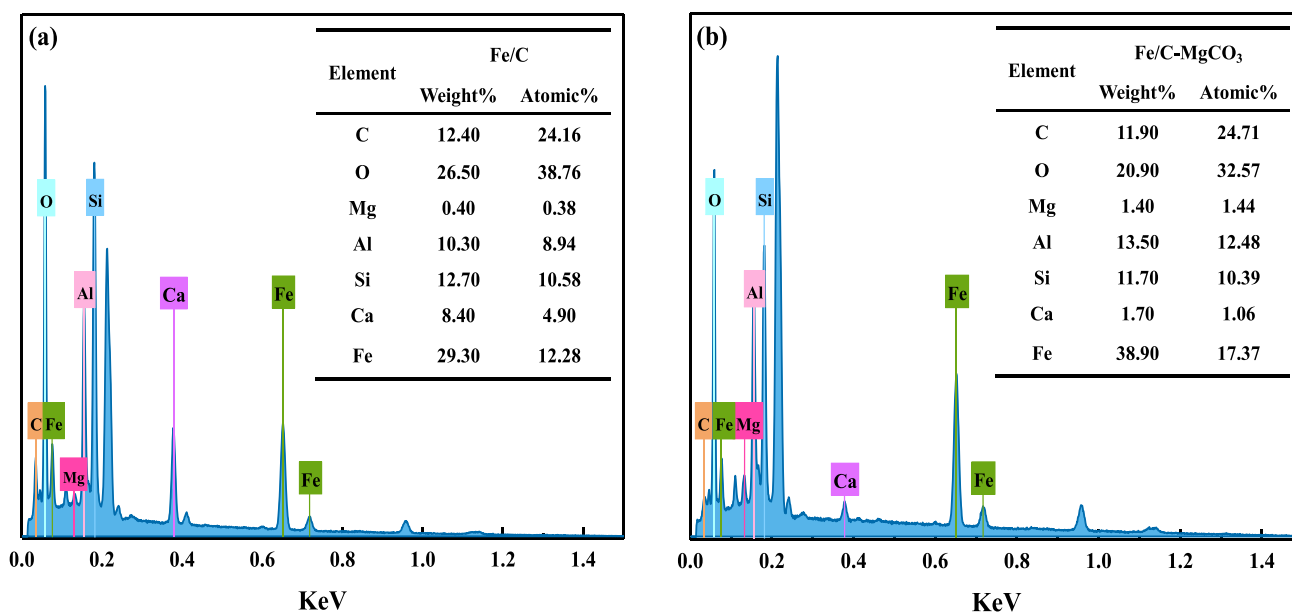


**Fig. 7** Energy-dispersive spectrometry (EDS) diagram of **a** Fe/C and **b** Fe/C-MgCO<sub>3</sub> (insert table: element composition of filler)

magnesium, iron, and calcium effectively combined with PO<sub>4</sub><sup>3-</sup> to remove phosphorus from wastewater.

The magnesium content on the filler surface increased after the addition of MgCO<sub>3</sub> (Fig. 7b). This indicated that the adherent on the filler surface might be MgCO<sub>3</sub> or MgO, and the results confirmed the prediction of the adherence made via SEM.

### Comparison of phosphorus removal processes

To further investigate the advantages of IC-ME using Fe/C-MgCO<sub>3</sub> as fillers to remove phosphorus from wastewater, the efficiencies, treatment mechanisms, advantages, and limitations of commonly used biological (Park et al. 2009) and physicochemical (Yang et al. 2010) methods for phosphorus removal are presented in Table 6.

Biological phosphorus removal processes have a wide range of applications and low cost. However, phosphorus removal using biological processes alone cannot meet increasingly stringent emission standards (Ren et al. 2020). In addition, the sludge yield of the biological method is large. Therefore, in order to meet strict emission standards, physicochemical phosphorus removal methods are often used after biological treatment (Ren et al. 2020).

Physicochemical phosphorus removal methods mainly include coagulation precipitation, adsorption, magnesium ammonium phosphate (MAP) precipitation, and IC-ME. The basic principle of the coagulation sedimentation is to add chemicals into the wastewater, then react with phosphate root to generate insoluble phosphate, and finally remove phosphorus in the wastewater through solid-liquid

separation. However, it has disadvantages of high cost and large dosage of phosphorus removal (Peng et al. 2018). The low adsorption capacity and high replacement cost of adsorbents make it difficult for adsorption phosphorus removal methods to be widely used (Li et al. 2021c). In the phosphorus removal process of MAP precipitation, solution pH is one of the most influential parameters. Dissolved phosphate exhibits different states (PO<sub>4</sub><sup>3-</sup>, HPO<sub>4</sub><sup>2-</sup>, H<sub>2</sub>PO<sub>4</sub><sup>-</sup>, H<sub>3</sub>PO<sub>4</sub>) under different pH conditions; therefore, pH affects the supersaturation of the substance (Peng et al. 2018). Studies have shown that pH adjustment is an important part of the phosphorus removal process by MAP precipitation (Nelson et al. 2003; Rahman et al. 2014).

The IC-ME has been widely used in phosphorus removal due to its characteristics of treating waste with waste and the raw materials are cheap and easy to obtain. Since the suitable working environment of the micro-electrolysis system is acidic, it is necessary to adjust the pH value in the early stage to exert its high efficiency (Yang et al. 2017), which is also an important part of the efficient phosphorus removal of IC-ME. The disadvantage of fillers that are easily hardened and passivated in traditional methods can be improved by modifying fillers (Li et al. 2021b). It can be seen from Table 6 that by adding metal elements to traditional fillers, the number of primary cells in the micro-electrolysis system can be increased, and the reaction efficiency can be enhanced. Commonly added metal elements are Al (Yang et al. 2016), Mg (Gao et al. 2022), and Ca (Ma et al. 2022). But metal Al is chemically active and easy to oxidize and form metal oxides. When the element Ca is added, the phosphorus removal efficiency is

**Table 6** Comparison of phosphorus removal processes

Method	Technology	Function	Removal rate	Mechanism	Advantage	Limitation
Biological methods	Traditional biological method	Excessive phosphorus uptake by phosphorus removal bacteria;	TP: 66.3%		Wide range of applications; Lower cost; Better treatment effect for low concentration of P.	Large output of sludge; High environmental requirements; It should be used simultaneously with the chemical method in practical application
	New biological method	Phosphorus release from phosphorus removal bacteria; Discharge of phosphorus-rich sludge (Zhao et al. 2022)	TP: >90%			
Physico-chemical method	Coagulation sedimentation method (Zhang et al. 2022)	Adding metal salts which could react with phosphorus in the water to generate insoluble or insoluble phosphate precipitates	TP: >96%		Easy to use; High phosphorus removal efficiency and stability; Strong impact resistance	Single contaminant removal; The consumption of phosphorus removal agents is large; High operation and maintenance costs
	Adsorption method (Lv et al. 2022)	Adsorption of phosphorus in wastewater by solid matter with pores and large specific surface area			Applicable to many water bodies; Fast adsorption rate; The adsorbent is recyclable	The adsorption saturation effect is decrease; Analytical waste liquid is difficult to handle
	Crystallization (Schott et al. 2022)	Add OH <sup>-</sup> to the wastewater containing calcium to form hydroxyl HAP crystals; Add Mg <sup>2+</sup> to the wastewater containing NH <sub>4</sub> <sup>+</sup> to form MAP crystals			High phosphorus removal efficiency; No secondary pollution; Easy to use; Wide range of applications	High cost of medicines; Applicable to high-concentration phosphorus content sewage
	Traditional Fe/C microelectrolytic filler (Yang et al. 2017)	In the absence of electricity, the micro electrolytic materials filled in the wastewater can produce a 1.2 V potential difference to conduct electrolytic treatment of the wastewater and achieve the degradation of pollutants	TP: 76%		Use waste to cure waste; Raw materials are readily available	Processing efficiency is not stable; Filler passivation
	Modified Fe/C micro electrolytic filler	Fe/C-Al (Yang et al. 2016)	TP: --		Iron and carbon integration; Large specific surface area; High stability;	Easy oxidation
		Fe/C-Mg (Gao et al. 2022) (Zhang et al. 2021)	TP: 98.6%		Avoiding passivation and compaction of packing during operation	Operational risk
		Fe/C-MgCO <sub>3</sub> (This work)	TP: >97%			pH adjustment
		Fe/C-CaCO <sub>3</sub> (Ma et al. 2022)	TP: >73%			Lower phosphorus removal efficiency

low. Since metal Mg easily reacts with water to generate hydrogen, excess metal Mg has a high safety risk factor (Gao et al. 2022).

Although the IC-ME using the self-made Fe/C-MgCO<sub>3</sub> as filler in this study has the same shortcomings as the conventional IC-ME which needs to adjust the pH value, it has the following advantages: (1) the addition of MgCO<sub>3</sub> to the filler significantly improves the phosphorus removal efficiency; (2) the participation of MgCO<sub>3</sub> increases the pH of the solution after the micro-electrolysis reaction and reduces the operating cost; (3) compared with the metal Mg modified filler, which is easy to generate hydrogen, the operation is safer; (4) the MAP formed in the reaction process can also be recycled and used as a potential raw material for the chemical fertilizer process, which can save economic costs. Therefore, the IC-ME process using Fe/C-MgCO<sub>3</sub> as filler will be a phosphorus removal process with industrial application prospects.

## Continuous run of the micro-electrolysis reactor

The micro-electrolysis reactor was operated continuously for 15 days under optimum parameters (influent pH of 3, HRT of 120 min, and aeration rate of 0.2 m<sup>3</sup>/h) and samples were taken according to the predetermined time intervals.

The running state of the micro-electrolysis reactor is illustrated in Fig. 8. During the continuous IC-ME process, the removal rates of TP, COD, and NH<sub>4</sub><sup>+</sup>-N by the Fe/C-MgCO<sub>3</sub> filler exhibited fluctuations. Thus, the experimental results can be divided into two parts based on the changes in removal rates of TP, COD, and NH<sub>4</sub><sup>+</sup>-N.

In the first part of the process, that is, the first 3 days of micro-electrolysis reactor operation, the removal rates of COD, TP, and NH<sub>4</sub><sup>+</sup>-N decreased to 51%, 85.5%, and 34.3%, respectively. During aeration at a low pH, the O<sub>2</sub> on the carbon cathode was reduced to oxygen free radicals (O·), reactive hydrogen, and hydrogen peroxide (H<sub>2</sub>O<sub>2</sub>), leading to the

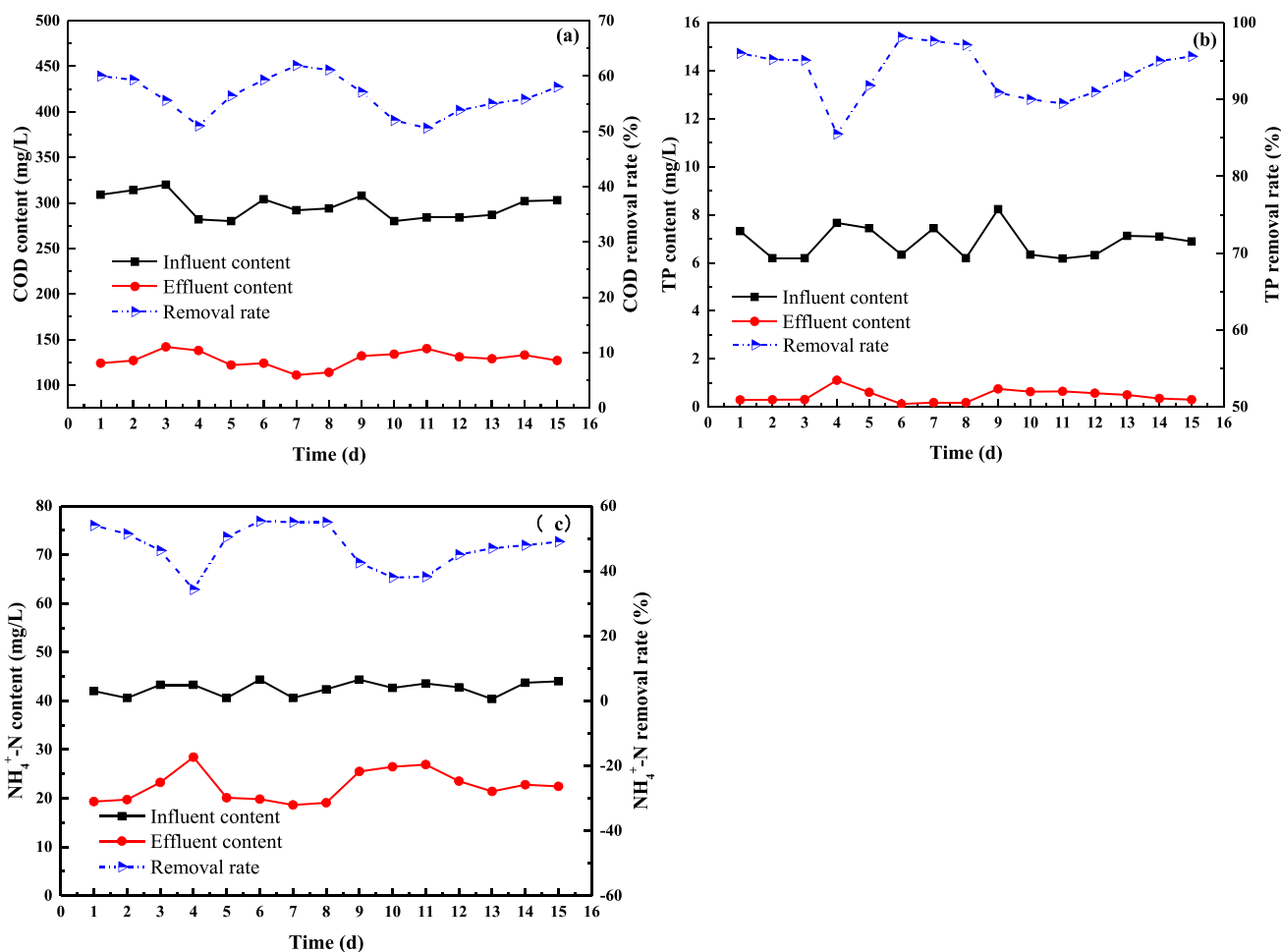


**Fig. 8** Successive running of the micro-electrolysis reactor (influent pH of 3, HRT of 120 min, and ventilation rate of 0.2 m<sup>3</sup>/h)

degradation of COD (Han et al. 2019). The contact between the Fe/C-MgCO<sub>3</sub> filler and pollutants was hindered by the passivation of iron on the filler surface and accumulation of other deposits such as corrosion products. In the second part of the process, the rate of removal gradually stabilized after increasing as the operation time lengthened from 3 to 8 days. This may be because, during the continuous aeration, the sediment layer increased to a specific thickness, and the scouring of gas, water flow, and collision between the fillers removed the sediment layer on the surface of the filler (Huang et al. 2014). Therefore, more active sites and structures were exposed on the surface of the filler which enhanced the contact between the filler and contaminants.

SEM and BET were used to test the surface morphology and specific surface area of the Fe/C-MgCO<sub>3</sub> filler to confirm the renewal of the filler surface (Figs. 9 and 10, and Table 7).

Figure 9a and Table 7 demonstrate that the surface of the Fe/C-MgCO<sub>3</sub> filler is rough and has an irregular shape because there are many small apertures on the surface that could enhance the specific surface area. After 3 days of continuous reaction experiments, the pore structure was blocked and micropore area was markedly reduced (Fig. 9b). This may be due to the deposition of iron oxides, iron hydroxides, and phosphorus reactants on the surface of the filler during the IC-ME process.

The specific surface area, micropore volume, and micropore area of the fillers increased significantly after the reaction was performed for 6 days (Fig. 9c and Table 7). The Fe/C-MgCO<sub>3</sub> filler surface became porous again due to the shedding of deposits from the filler surface. When

the reaction proceeded to the 9th day, the pore structure on the filler surface was blocked by sediment again (Fig. 9d). The deposited layer may possibly be shed again after a specific operating time and renewal of the filler surface. Thus, a cyclic renewal process occurred which led to the continuous removal of phosphorus in wastewater.

The adsorption–desorption isotherm diagram and pore size distribution diagram with the application of the fillers are shown in Fig. 10. All four fillers exhibited distinct peaks in the range of 3–5 nm. As the operating time is extended, a fluctuating trend of first decreasing, increasing thereafter, and subsequently decreasing is evident that further proves the analysis results of SEM.

After continuous operation, the Fe/C-MgCO<sub>3</sub> packing was removed from the reactor, and no adhesion was observed between the packings, indicating that the Fe/C-MgCO<sub>3</sub> packing could effectively prevent the packing from hardening.

To investigate the long-term effect of removing TP from actual wastewater, the micro-electrolysis reaction formed by the Fe/C-MgCO<sub>3</sub> filler prepared in this study was applied to the treatment of landfill leachate. The operation time was 10 days. For comparison, the micro-electrolysis processes using conventional fillers were also applied to the treatment of actual landfill leachate under the same operating conditions. Figure 11 shows the effect of long-term phosphorus removal by micro-electrolysis using different fillers on actual landfill leachate.

The results indicate that the removal of TP from actual landfill leachate by micro-electrolysis, formed by Fe/C-MgCO<sub>3</sub> filler, exhibited a trend of fluctuation and slow

**Fig. 9** Scanning electron microscopy (SEM) images of the surfaces of the fillers: **a** 0 days; **b** 3 days; **c** 6 days; and **d** 9 days

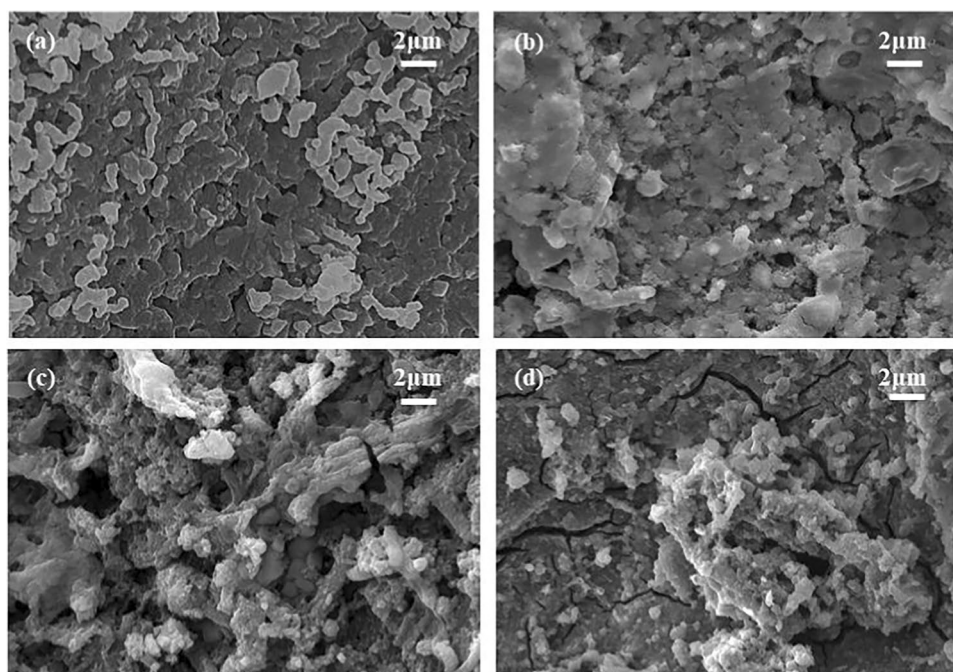




**Fig. 10** Pore size distribution of packing (insert image: adsorption–desorption (AD) isotherms)

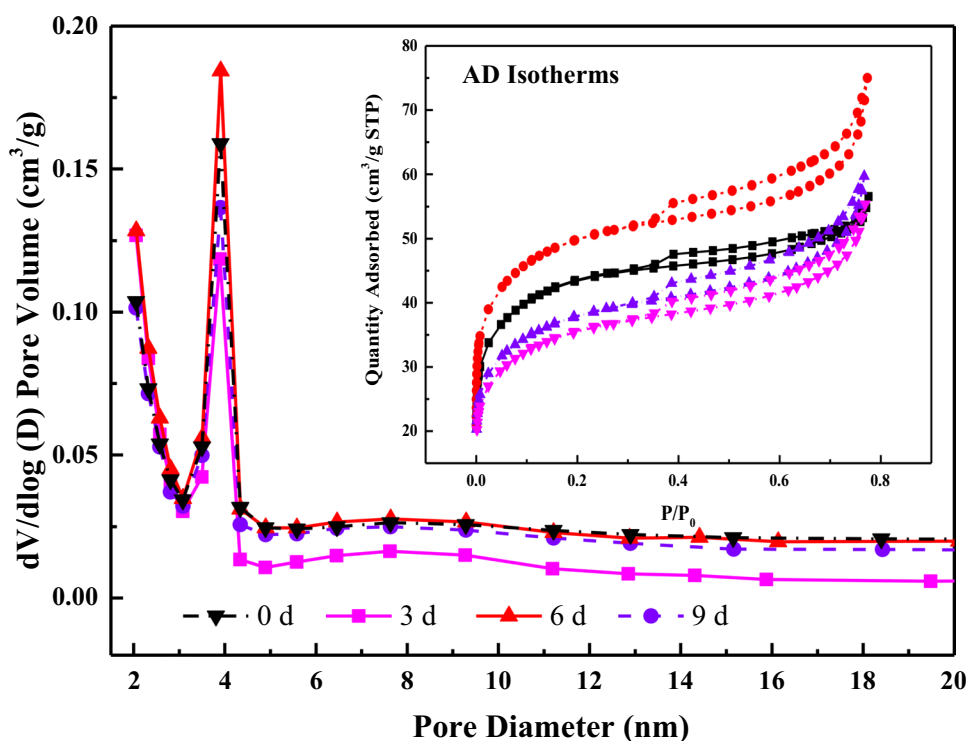


**Table 7** Brunauer–Emmett–Teller (BET) analysis for packing

Physical parameters	0 days	3 days	6 days	9 days
Specific surface area (m <sup>2</sup> /g)	154.23	124.96	177.04	133.51
Langmuir surface area (m <sup>2</sup> /g)	207.89	175.95	241.24	187.86
Micropore volume (cm <sup>3</sup> /g)	0.03	0.02	0.04	0.02
Micropore area (m <sup>2</sup> /g)	71.06	52.45	84.99	57.72
External surface area (m <sup>2</sup> /g)	83.17	72.52	92.05	75.79

decline within 10 days of continuous operation, and a stable removal rate exceeding 60%. However, the removal rate of TP by micro-electrolysis formed by traditional fillers was greatly reduced. As the TP removal rate fluctuation for simulated wastewater corresponds with the renewal of the Fe/C-MgCO<sub>3</sub> filler surface shown by SEM test results, the removal rate fluctuation may be mainly caused by the periodic renewal of the filler surface. Because of the complex composition of actual wastewater, the formation of sediments on the filler surface and the frequency of surface detachment and renewal were faster than for simulated wastewater. Therefore, the fluctuating form of the removal rate exhibited a different frequency compared to the simulated wastewater.

The two packings in the reactor were observed after 10 days of continuous operation; the traditional micro-electrolysis packings formed small agglomerates, whereas the Fe/C-MgCO<sub>3</sub> packings maintained a relatively independent integrity. During the long-term continuous operation of the traditional micro-electrolytic fillers, a high-density

passivation film formed on the iron surface. Moreover, the passivation film coverage reduced the specific surface area of the iron and carbon, hindered the contact between the iron and carbon, and reduced the galvanic effect. Consequently, the TP removal rate decreased significantly. Compared with traditional micro-electrolytic fillers, Fe/C-MgCO<sub>3</sub> fillers are conventional micro-electrolytic fillers prepared by high-temperature roasting technology applied to a clay skeleton. The addition of clay separates the iron filings with strong activity and also ensures effective contact between the iron and activated carbon. The long-term continuous operation results demonstrate that the Fe/C-MgCO<sub>3</sub> filler is characterized by automatic surface renewal, and has a longer stable operation period and higher TP removal rate.

## Mechanism of phosphorus removal of the modified Fe/C-MgCO<sub>3</sub> filler

### Surface morphologies of Fe/C-MgCO<sub>3</sub>

The surface morphology of the Fe/C-MgCO<sub>3</sub> filler after wastewater treatment was compared with that of the original filler using SEM characterization to elucidate the phosphorus removal mechanism in this study (Fig. 12a and b). The filler surface was rough and porous, and certain particles were tightly embedded in the filler surface, as illustrated by Fig. 12a. This increased the probability of



**Fig. 11** Long-term phosphorus removal effect of micro-electrolysis with different fillers on actual landfill leachate

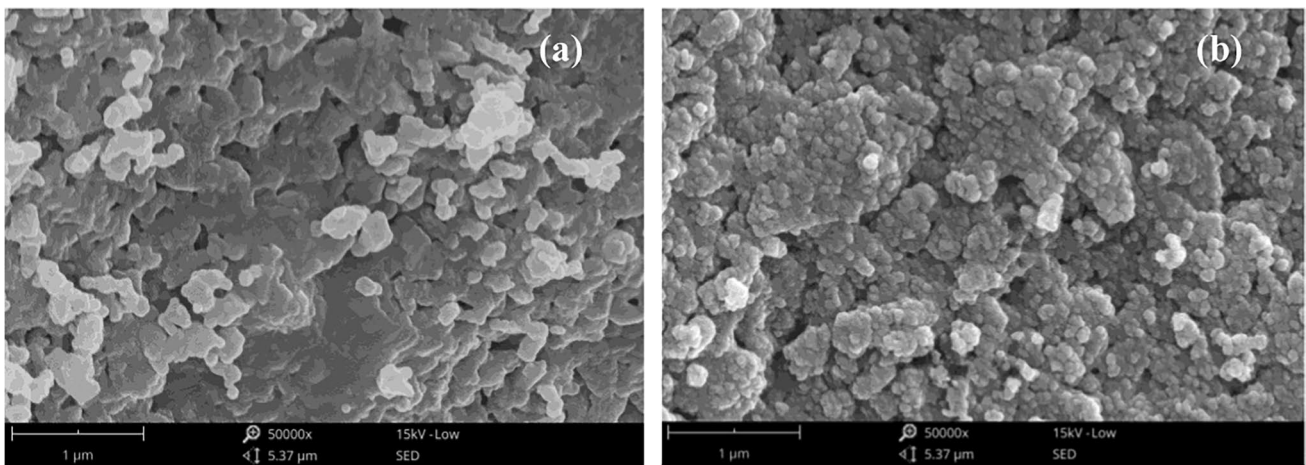
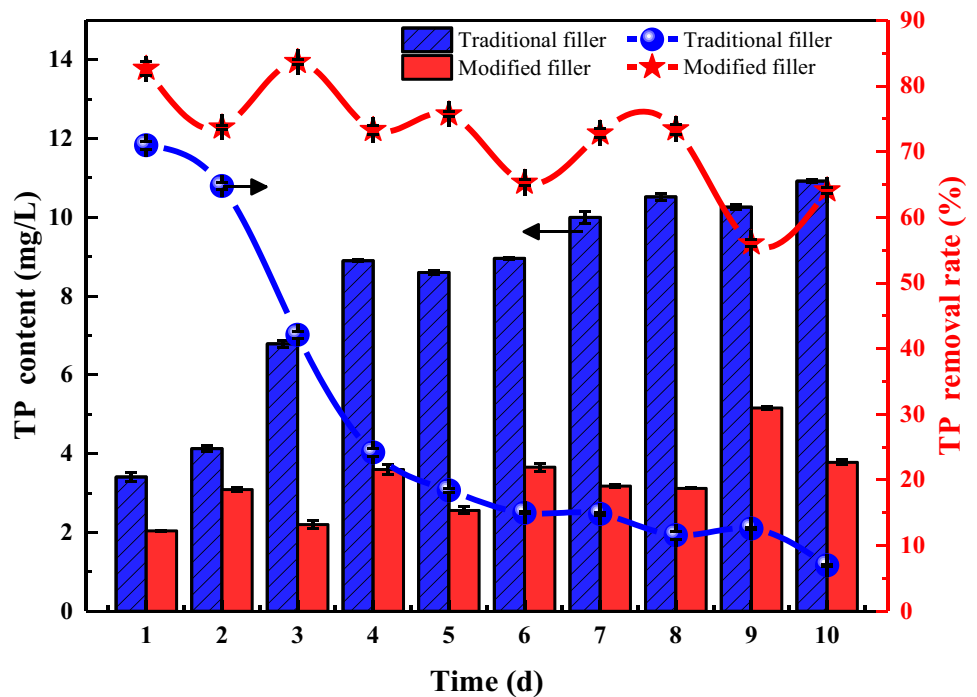


**Fig. 12** Scanning electron microscopy (SEM) images of modified micro-electrolytic fillers: **a** before the reaction, and **b** after the reaction. Magnification: 5000×

contact between the reactant and active sites of the fillers, and thus promoted the reactivity of the fillers.

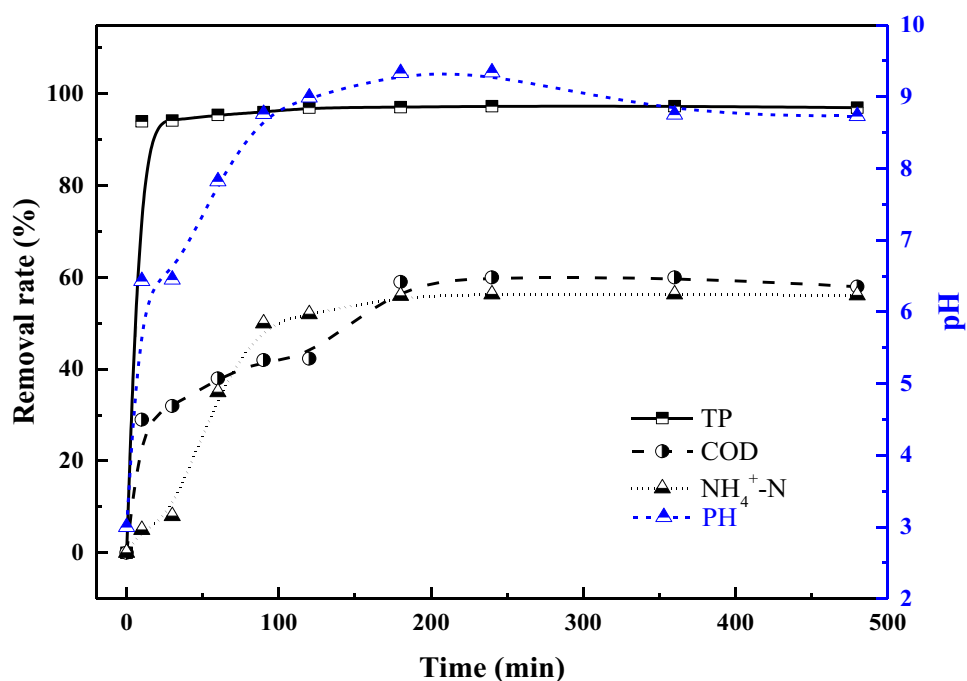
After phosphorus wastewater treatment, the particulate matter disappeared, and many fine spherical clusters appeared. This phenomenon has been reported with respect to the adsorption system using natural calcium-rich attapulgite as the adsorbent for phosphorus removal (Yin and Kong 2014). The fine spherical clusters could be attributed to the precipitates that resulted from the complex chemical reactions of Mg, Fe, and P (Li et al. 2017).

### Surface chemical property analysis of the Fe/C-MgCO<sub>3</sub> filler

To clarify the mechanism of phosphate removal from the Fe/C-MgCO<sub>3</sub> filler, the variation in pH of the solution and Fe/C-MgCO<sub>3</sub> filler structure was investigated during the reaction process. The change in pH of the solution and removal rate over time was studied (Fig. 13).

In the initial stage of the reaction, the pH of the solution increased rapidly over time. This behavior was attributed

**Fig. 13** Change in pH of the solution and removal rate during the reaction process



to the rapid protonation of MgO on the filler surface (Zhu et al. 2020) and participation of H<sup>+</sup> in the redox reaction to generate H<sub>2</sub>, thereby decreasing the concentration of H<sup>+</sup> and increasing the pH of the solution.

The next stage was the rapid reaction stage wherein the pH of the solution gradually reached the maximum value. This behavior was attributed to the oxidation of Fe<sup>2+</sup> to Fe<sup>3+</sup> by aerobic aeration, which increased the pH of the solution (Yang et al. 2017). In this stage, the main form of phosphate present was H<sub>2</sub>PO<sub>4</sub><sup>-</sup> (pH ranged from 3 to 7.8) (Liu et al. 2021b). Because of the action of the following reaction, NH<sub>4</sub><sup>+</sup> + H<sub>2</sub>PO<sub>4</sub><sup>-</sup> + Mg<sup>2+</sup> + 6H<sub>2</sub>O = MgNH<sub>4</sub>PO<sub>4</sub>•6H<sub>2</sub>O + 2H<sup>+</sup>, the removal rate of NH<sub>4</sub><sup>+</sup>-N reflected an upward trend in this stage (Mehta and Batstone 2013). Under acidic conditions, the cathode reaction of the filler consumed H<sup>+</sup>, which further promoted struvite formation. The last stage was characterized by a drop in pH, resulting from two main reasons: (a) the OH<sup>-</sup> in the solution was consumed because of the precipitation of Fe(OH)<sub>3</sub>; and (b) the precipitation of struvite resulted in a rapid decrease in pH according to the following reaction, NH<sub>4</sub><sup>+</sup> + HPO<sub>4</sub><sup>2-</sup> + Mg<sup>2+</sup> + 6H<sub>2</sub>O = MgNH<sub>4</sub>PO<sub>4</sub>•6H<sub>2</sub>O + H<sup>+</sup>, indicating that HPO<sub>4</sub><sup>2-</sup> rather than PO<sub>4</sub><sup>3-</sup> was involved in the struvite formation reaction (Hao et al. 2008).

The experimental results indicate that the rate of TP removal remains at an elevated level under higher pH conditions. The disadvantage of low efficiency of the IC-ME reaction in a high pH environment decreases, that is, the efficiency of the IC-ME reaction improves, and the pH range of the IC-ME reaction broadens.

The XPS spectra and XRD measurements of the Fe/C-MgCO<sub>3</sub> filler before and after the phosphorus removal

reaction were also analyzed to understand the phosphorus removal mechanism. Figure 14a illustrates that before the phosphorus removal reaction, Fe/C-MgCO<sub>3</sub> revealed the peaks of Fe 2p, O 1s, C 1s, and Mg 1s at 711.8, 530.05, 284.1, and 1304.4 eV, respectively. After the reaction, the P 2p peaks of Fe/C-MgCO<sub>3</sub> at 133.7 and 134.9 eV (Fig. 14b) were attributed to PO<sub>4</sub><sup>3-</sup> and HPO<sub>4</sub><sup>2-</sup>, respectively (Liu et al. 2021a; Xie et al. 2014). The appearance of the P 2p peak after phosphorus removal proved that phosphate was successfully loaded onto the Fe/C-MgCO<sub>3</sub> filler; thus, the surface of the modified filler was composed of PO<sub>4</sub><sup>3-</sup> and HPO<sub>4</sub><sup>2-</sup>. These phosphorus species were predominately associated with Fe<sup>2+</sup>, Fe<sup>3+</sup>, and Mg<sup>2+</sup>, which led to Mg-P and Fe-P precipitation (Zhou et al. 2020).

Figure 14c illustrates the Fe 2p XPS spectra of Fe/C-MgCO<sub>3</sub> before the phosphorus removal. A satellite peak at ≈ 718.9 eV, along with the doublet of 2p<sub>3/2</sub> and 2p<sub>1/2</sub> at ≈ 712.3 and ≈ 723.5 eV, respectively, was evident for Fe<sup>3+</sup> (Xu et al. 2018), whereas the peak at ≈ 710.7 eV was assigned to Fe<sup>2+</sup>. These two main characteristic peaks indicate the presence of iron oxide on the surface of the composite packing, either in the form of FeO or Fe<sub>2</sub>O<sub>3</sub>; these may be attributed to the failure of the composite packing to completely isolate O<sub>2</sub> during the roasting process, leading to partial oxidation on its surface (Li and Zhang 2007). After the reaction, a chemical shift of 1.6 eV was observed for Fe 2p<sub>1/2</sub> although the 2p<sub>3/2</sub> did not show a shift. The spectrum of Fe 2p after the phosphorus removal reaction is illustrated in Fig. 14d. The Fe 2p peaks at 725.1 and 711.8 eV were attributed to Fe 2p<sub>1/2</sub> and Fe 2p<sub>3/2</sub> of FePO<sub>4</sub>, respectively (Tan 2016).

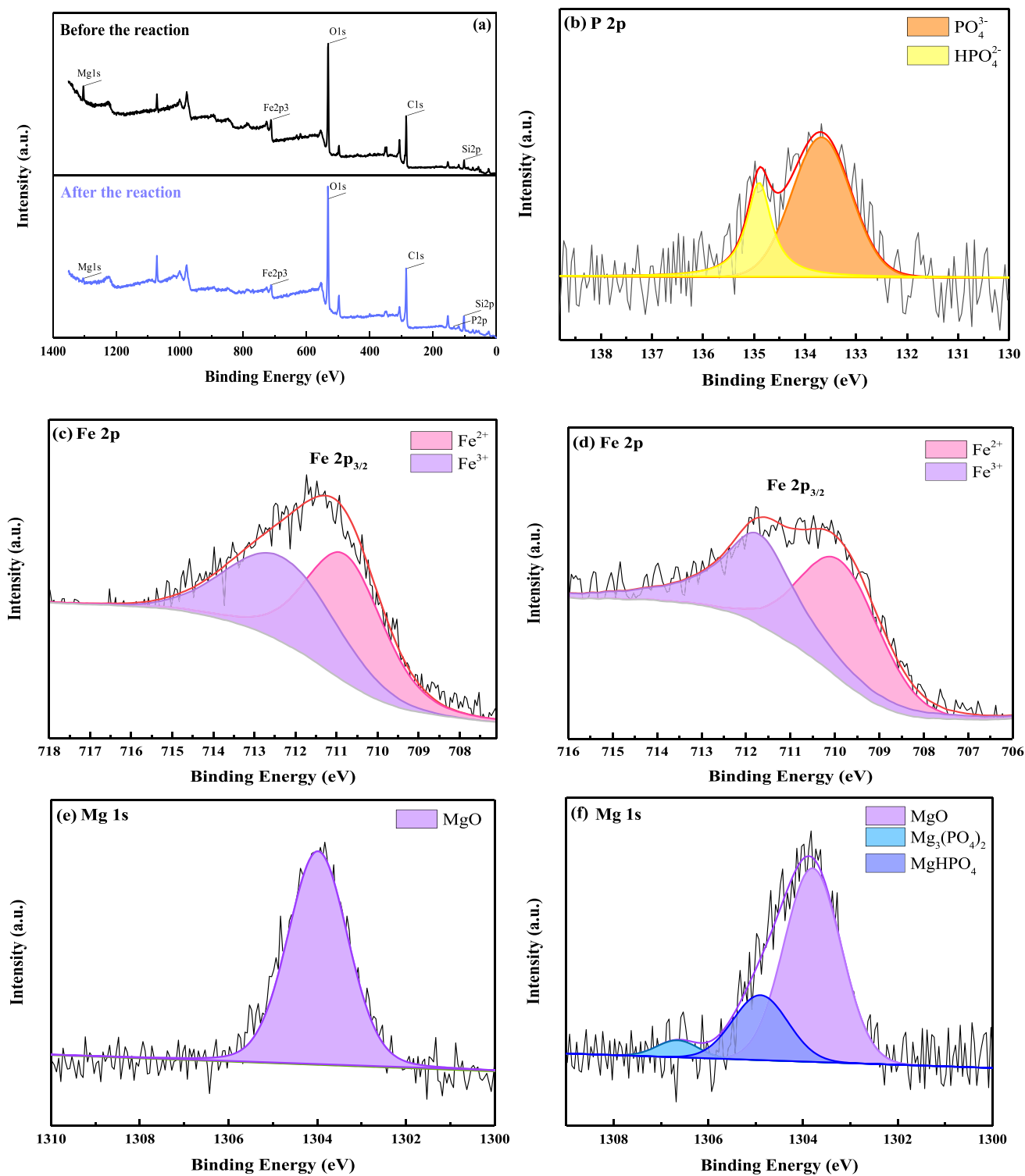


**Fig. 14** a High-resolution spectra of X-ray photoelectron spectroscopy (XPS) analyses of Fe/C- $\text{MgCO}_3$  before and after the reaction; b P 2p after the reaction; c, d Fe 2p; e, f Mg 2p

There were significant changes observed for the Mg 1s of Fe/C- $\text{MgCO}_3$  before and after the reaction. Magnesium was present predominantly as MgO before the reaction.

After the reaction, the MgO peak was still present; however, the peak area had decreased markedly and the characteristic peaks of  $\text{MgHPO}_4$  and  $\text{Mg}_3(\text{PO}_4)_2$  appeared. These

results indicate that MgO was involved in the phosphorus removal reaction and possibly converted to  $\text{MgHPO}_4$  and  $\text{Mg}_3(\text{PO}_4)_2$  (Liu et al. 2021a; Zhu et al. 2020).

Figure 15a illustrates the XRD spectra of Fe/C-MgCO<sub>3</sub> before and after the phosphorus removal reaction. The main crystal phases of Fe/C-MgCO<sub>3</sub> before the reaction were Fe, FeO, Fe<sub>2</sub>O<sub>3</sub>, Fe<sub>3</sub>O<sub>4</sub>, SiO<sub>2</sub>, and MgO. After the removal of phosphorus using Fe/C-MgCO<sub>3</sub>, the characteristic peaks of FePO<sub>4</sub> for this filler appeared at 43.3, 61.4, and 61.6 of 2θ, and those of Mg<sub>3</sub>(PO<sub>4</sub>)<sub>2</sub> appeared at 29.8, 32.0, 42.4, and 61.6 of 2θ. The characteristic peaks of MgHPO<sub>4</sub> appeared at 28.9, 35.5, 43.7, and 51.8 of 2θ, indicating that the phosphate in water reacted with the iron and magnesium in Fe/C-MgCO<sub>3</sub>.

The sediments obtained during the optimum conditions were used for the analysis of the crystalline mineral facies; when compared with the standard pattern, the Jade software had strong diffraction peaks at 14.04°, 21.04°, 27.22°, 36.38°, and 46.41°. The peaks of struvite indicated that struvite was the main phase present. FePO<sub>4</sub>, MgHPO<sub>4</sub>, and Mg<sub>3</sub>(PO<sub>4</sub>)<sub>2</sub> were also identified as minor phases present in the sediments. The identity of the other phases present in small quantities was very difficult to establish, because the pattern is characterized by numerous small overlapping peaks (Chimenos et al. 2003).

According to these results, a reaction mechanism is proposed to illustrate the removal of phosphates using MgCO<sub>3</sub> as the magnesium source (Zhang et al. 2009).

## Fe/C-MgCO<sub>3</sub> filler phosphorus removal mechanism diagram

The reaction of conventional IC-ME in the presence of oxygen mainly includes the oxidation of iron to form Fe<sup>2+</sup> (Eq. (2)) and Fe<sup>3+</sup> (Eq. (3)) (Han et al. 2016, 2019, 2020), which simultaneously enhance the production of Fe(OH)<sub>2</sub> and Fe(OH)<sub>3</sub>, respectively. The contaminants in wastewater can be removed indirectly by co-precipitation and the enmeshment of ferrous and ferric hydroxide floc. Fe<sup>3+</sup> on the surface of the filler or in the solution reacts easily with PO<sub>4</sub><sup>3-</sup> to precipitate FePO<sub>4</sub> (Eq. (4)) (Thistleton et al. 2002), as confirmed by the XRD results. At high temperatures, the MgCO<sub>3</sub> in the Fe/C-MgCO<sub>3</sub> filler in this study easily produced MgO that could combine with H<sup>+</sup> on the surface of the filler to form a protonated MgOH<sup>+</sup> (Eq. (5)) (Watanabe et al. 1995). The phosphate has a negative charge. The protonated MgOH<sup>+</sup> has a positive charge and can be adsorbed by electrostatic attraction to form a surface complex, namely MgOH-HPO<sub>4</sub> (Eq. (6)) (Shu et al. 2019), and lose a hydroxyl ion to form MgHPO<sub>4</sub> (Eq. (7)), or lose additional water molecules to form Mg<sub>3</sub>(PO<sub>4</sub>)<sub>2</sub> (Eq. (8)) (Zhu et al. 2020). This can be confirmed by the XRD and XPS results. The XRD results illustrate that the Mg<sup>2+</sup> released into the solution can combine with H<sub>2</sub>PO<sub>4</sub><sup>-</sup>, HPO<sub>4</sub><sup>2-</sup>, PO<sub>4</sub><sup>3-</sup>, and NH<sub>4</sub><sup>+</sup> to form struvite (MgNH<sub>4</sub>PO<sub>4</sub>·6H<sub>2</sub>O) (Eqs. (9–11)) (Rabinovich et al. 2021) and to form a precipitate upon deposition. Therefore, a possible phosphorus removal mechanism is shown in Fig. 16.

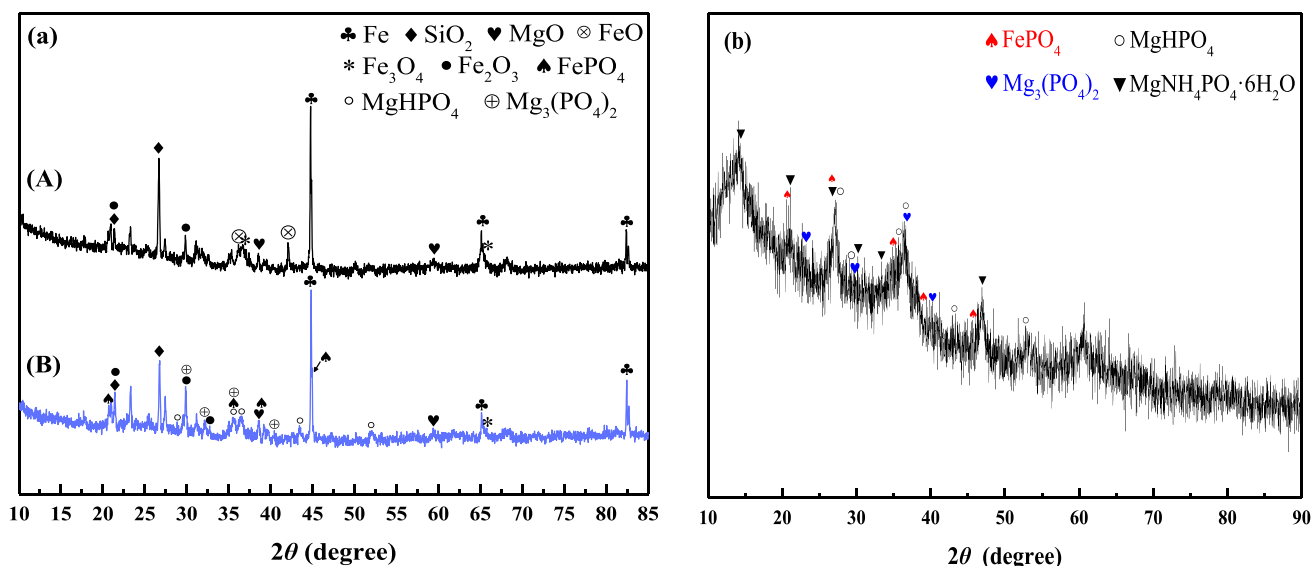


**Fig. 15** X-ray diffraction (XRD) patterns of Fe/C-MgCO<sub>3</sub> (A) before and (B) after the phosphorus removal reaction (a); XRD patterns of the sediments after reaction (b)



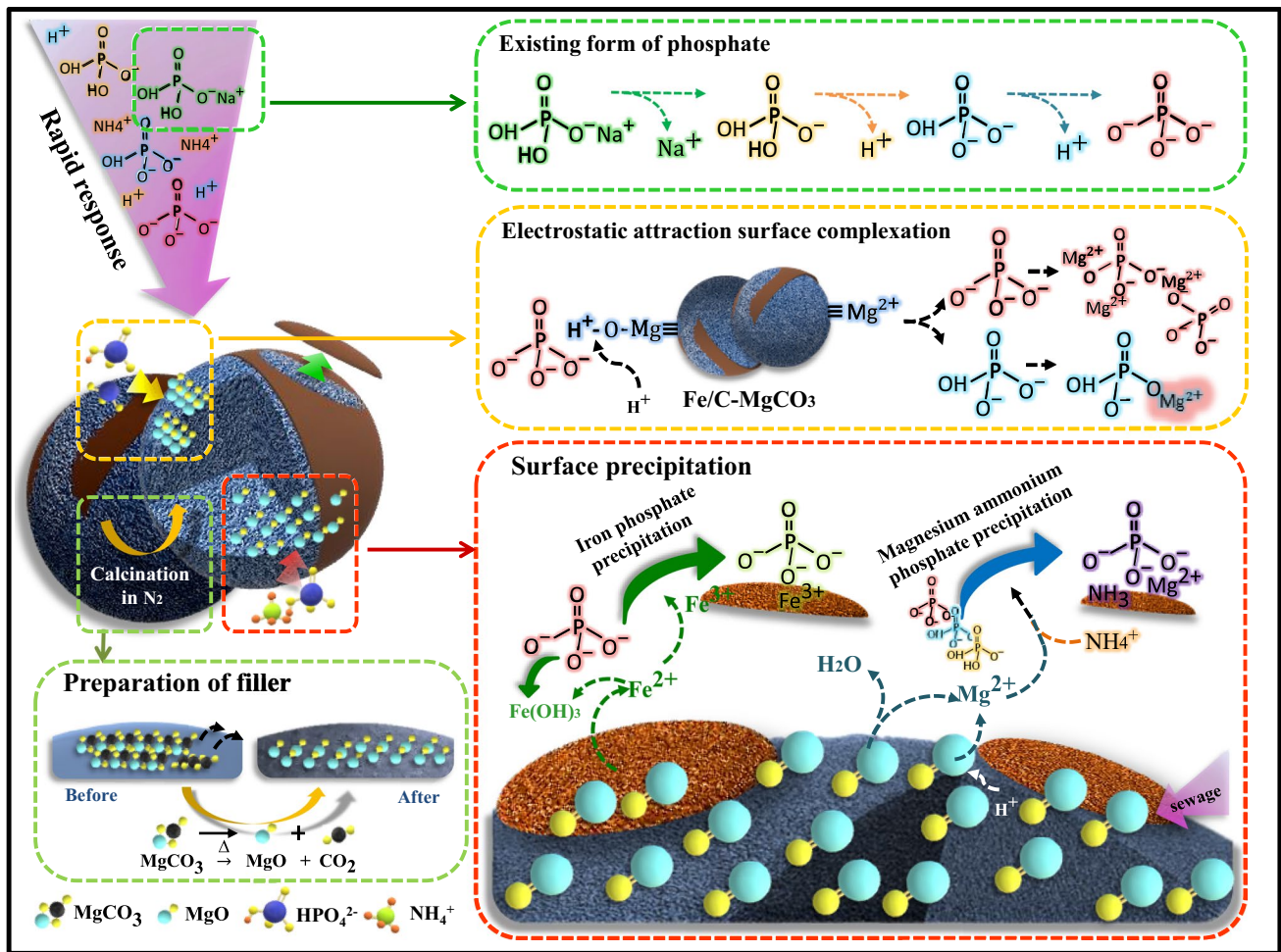
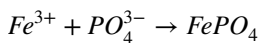
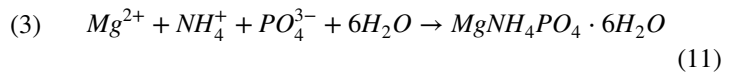
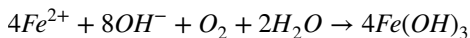
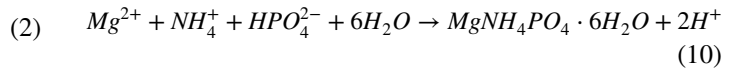
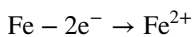
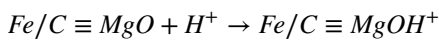


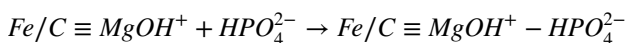
Fig. 16 Schematic diagram of the mechanism of phosphorus removal in iron-carbon micro-electrolysis (IC-ME)



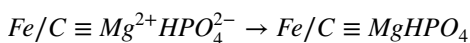
(4)



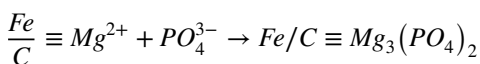
(5)



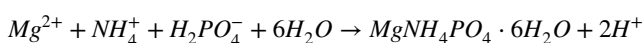
(6)



(7)



(8)



(9)

### Conclusion

In this study, magnesium metal oxides were successfully utilized to prepare the Fe/C-MgCO<sub>3</sub> filler, and the preparation conditions were optimized for efficient phosphorus removal. The phosphorus removal mechanism was investigated via the IC-ME process using the Fe/C-MgCO<sub>3</sub> filler. The optimum conditions for preparing the modified micro-electrolytic fillers were a calcination temperature of 800 °C, Fe/C ratio of 4:1, clay content of 20%, and additive content of 5%. Under the optimum preparation conditions determined by single-factor experiments, the phosphorus removal rate was 97%, and the Fe/C-MgCO<sub>3</sub> filler with a compressive



strength of 3.5 MPa and a specific surface area of 154.2 m<sup>2</sup>/g met the standards of artificial ceramsite filter materials for water treatment. SEM–EDS, XRD, and XPS analyses indicate that the removal of phosphorus from water involved simultaneous processes of electrostatic adsorption and surface precipitation to form the major products, namely, MgNH<sub>4</sub>PO<sub>4</sub>·6H<sub>2</sub>O, MgHPO<sub>4</sub>, Mg<sub>3</sub>(PO<sub>4</sub>)<sub>2</sub>, and FePO<sub>4</sub>. The Fe/C–MgCO<sub>3</sub> filler demonstrated the ability to remove phosphorus substantially and appears to be a promising filler for the removal of phosphate from wastewater.

**Acknowledgements** The authors are thankful for the support by the National Natural Science Foundation of China (grant number 21908008, 21677018), the Jointly Projects of Beijing Natural Science Foundation and Beijing Municipal Education Commission (grant number KZ201810017024), and Cross-Disciplinary Science Foundation from Beijing Institute of Petrochemical Technology (grant number BIPTCSF-22032205003/014).

**Author contribution** Yanhe Han: conceptualization, writing—review and editing, supervision, funding acquisition; Zhimin Su: methodology, investigation, formal analysis, writing—original draft; Xuejiao Ma: revising—review and editing, funding acquisition; Xiaolu Fu: investigation, formal analysis; Han Xu: investigation, formal analysis; Lina Liu: investigation, formal analysis; Meili Liu: revising—review and editing, funding acquisition.

**Funding** This work was supported by the National Natural Science Foundation of China (grant number 21908008, 21677018), the Jointly Projects of Beijing Natural Science Foundation and Beijing Municipal Education Commission (grant number KZ201810017024), and Cross-Disciplinary Science Foundation from Beijing Institute of Petrochemical Technology (grant number BIPTCSF-22032205003/014).

**Data availability** The metadata used and/or analyzed during the current study are available from the corresponding author upon reasonable request.

## Declarations

**Ethics approval** Not applicable.

**Consent to participate** All authors participated in this work.

**Consent to publish** All authors agree to publish.

**Competing interests** The authors declare no competing interests.

## References

- Barat R, Montoya T, Seco A, Ferrer J (2011) Modelling biological and chemically induced precipitation of calcium phosphate in enhanced biological phosphorus removal systems. *Water Res* 45:3744–3752. <https://doi.org/10.1016/j.watres.2011.04.028>
- Bi X, Guo L (2020) Treatment process of rural domestic sewage based on small purification tank technology. *IOP Con Ser: Earth Environ Sci* 450:012110. <https://doi.org/10.1088/1755-1315/450/1/012110>
- Chimenos JM, Fernández AI, Villalba G, Segarra M, Urruticoechea A, Artaza B, Espiell F (2003) Removal of ammonium and phosphates from wastewater resulting from the process of cochineal extraction using MgO-containing by-product. *Water Res* 37:1601–1607. [https://doi.org/10.1016/s0043-1354\(02\)00526-2](https://doi.org/10.1016/s0043-1354(02)00526-2)
- Devasahayam S, Strezov V (2018) Thermal decomposition of magnesium carbonate with biomass and plastic wastes for simultaneous production of hydrogen and carbon avoidance. *J Clean Prod* 174:1089–1095. <https://doi.org/10.1016/j.jclepro.2017.11.017>
- Gao P, Zhang Y, Wang S (2022) Increasing the hydrophyte removal rate of dissolved inorganic phosphorus using a novel Fe–Mg-loaded activated carbon hydroponic substrate with adsorption–release dual functions. *J Environ Manage* 313:114998. <https://doi.org/10.1016/j.jenvman.2022.114998>
- Guo WQ, Luo HC, Yang SS, Wu QL, Peng SM (2014) Emerging technologies for phosphorus removal and recovery: a review. *Appl Mech Mater* 507:702–706. <https://doi.org/10.4028/www.scientific.net/AMM.507.702>
- Han Y, Li H, Liu M, Sang Y, Liang C, Chen J (2016) Purification treatment of dyes wastewater with a novel micro-electrolysis reactor. *Sep Purif Technol* 170:241–247. <https://doi.org/10.1016/j.seppur.2016.06.058>
- Han Y, Qi M, Zhang L, Sang Y, Liu M, Zhao T, Niu J, Zhang S (2019) Degradation of nitrobenzene by synchronistic oxidation and reduction in an internal circulation microelectrolysis reactor. *J Hazard Mater* 365:448–456. <https://doi.org/10.1016/j.jhazmat.2018.11.036>
- Han Y, Zhang L, Liu M, Niu J (2020) Numerical simulation of the hydrodynamic behavior and the synchronistic oxidation and reduction in an internal circulation micro-electrolysis reactor. *Chem Eng J* 381:122709. <https://doi.org/10.1016/j.cej.2019.122709>
- Hao XD, Wang CC, Lan L, van Loosdrecht MC (2008) Struvite formation, analytical methods and effects of pH and Ca<sup>2+</sup>. *Water Sci Technol* 58:1687–1692. <https://doi.org/10.2166/wst.2008.557>
- Huang D, Yue Q, Fu K, Zhang B, Gao B, Li Q, Wang Y (2014): Application for acrylonitrile wastewater treatment by new micro-electrolysis ceramic fillers. *Desalin Water Treat*, 1–9. <https://doi.org/10.1080/19443994.2014.995717>
- Kang M, Chen Q, Li J, Liu M, Weng Y (2019a) Preparation and study of a new type of Fe–C microelectrolysis filler in oil-bearing ballast water treatment. *Environ Sci Pollut R* 26:10673–10684. <https://doi.org/10.1007/s11356-019-04480-z>
- Kang M, Chen Q, Li J, Liu M, Weng Y (2019b) Preparation and study of a new type of Fe–C microelectrolysis filler in oil-bearing ballast water treatment. *Environ Sci Pollut R* 26:10673–10684. <https://doi.org/10.1007/s11356-019-04480-z>
- Kong L, Xiong Y, Tian S, Luo R, He C, Huang H (2013) Preparation and characterization of a hierarchical porous char from sewage sludge with superior adsorption capacity for toluene by a new two-step pore-fabricating process. *Bioresour Technol* 146:457–462. <https://doi.org/10.1016/j.biortech.2013.07.116>
- Kong L, Tian Y, Wang Y, Li N, Liu Y, Pang Z, Huang X, Li M, Zhang J, Zuo W (2019) Periclase-induced generation of flowerlike clay-based layered double hydroxides: a highly efficient phosphate scavenger and solid-phase fertilizer. *Chem Eng J* 359:902–913. <https://doi.org/10.1016/j.cej.2018.11.007>
- Li XQ, Zhang WX (2007) Sequestration of metal cations with zerovalent iron nanoparticles: a study with high resolution X-ray photoelectron spectroscopy (HR-XPS). *J Phys Chem C* 111:6939–6946. <https://doi.org/10.1021/jp0702189>
- Li R, Wang JJ, Zhou B, Zhang Z, Liu S, Lei S, Xiao R (2017) Simultaneous capture removal of phosphate, ammonium and organic substances by MgO impregnated biochar and its potential use in swine wastewater treatment. *J Clean Prod* 147:96–107. <https://doi.org/10.1016/j.jclepro.2017.01.069>

- Li J, Ta N, Li Y, Shen W (2018) Morphology Effect of Nano-Scale CeO<sub>2</sub> in Heterogeneous Catalytic Reactions. *Chinese J Catal* 29:823–830
- Li P, Luo S, Zhang L, Wang Q, Huang X, Zhang Y, Liu X, Liang J, Duan X (2021a) Study on preparation and performance of iron tailings-based porous ceramsite filter materials for water treatment. *Sep Purif Technol* 276:119380. <https://doi.org/10.1016/j.seppur.2021.119380>
- Li X, Jia Y, Qin Y, Zhou M, Sun J (2021b) Iron-carbon microelectrolysis for wastewater remediation: preparation, performance and interaction mechanisms. *Chemosphere* 278:130483. <https://doi.org/10.1016/j.chemosphere.2021.130483>
- Li Y, Nan X, Li D, Wang L, Xu R, Li Q (2021c) Advances in the treatment of phosphorus-containing wastewater. *IOP Conference Series: Earth Environ Sci* 647:012163. <https://doi.org/10.1088/1755-1315/647/1/012163>
- Liu H, Li G, Qu J, Liu H (2007) Degradation of azo dye Acid Orange 7 in water by Fe<sup>0</sup>/granular activated carbon system in the presence of ultrasound. *J Hazard Mater* 144:180–186. <https://doi.org/10.1016/j.jhazmat.2006.10.009>
- Liu X, Feng Y, Li H (2011) Preparation of basic magnesium carbonate and its thermal decomposition kinetics in air. *J Cent South Univ* 18:1865–1870. <https://doi.org/10.1007/s11771-011-0915-z>
- Liu X, Fu J, Tang Y, Smith RL Jr, Qi X (2021a) Mg-coordinated self-assembly of MgO-doped ordered mesoporous carbons for selective recovery of phosphorus from aqueous solutions. *Chem Eng J* 406:126748. <https://doi.org/10.1016/j.cej.2020.126748>
- Liu X, Wang Y, Smith RL, Fu J, Qi X (2021b) High-capacity structured MgO-Co adsorbent for removal of phosphorus from aqueous solutions. *Chem Eng J* 426:131381. <https://doi.org/10.1016/j.cej.2021.131381>
- Lv N, Li X, Qi X, Y R (2022) Calcium-modified granular attapulgite removed phosphorus from synthetic wastewater containing low-strength phosphorus. *Chemosphere* 296. <https://doi.org/10.1016/j.chemosphere.2022.133898>
- Ma X, Gao L, Zhang Q, Hua W, Zhang Y, Li X, Yang J, Ding S, Hu C (2022) Nano-CaCO<sub>3</sub> templated porous carbons anchored with Fe single atoms enable high-efficiency N<sub>2</sub> electroreduction to NH<sub>3</sub>. *Electrochim Acta* 426:140805. <https://doi.org/10.1016/j.electacta.2022.140805>
- Mehta CM, Batstone DJ (2013) Nucleation and growth kinetics of struvite crystallization. *Water Res* 47:2890–2900. <https://doi.org/10.1016/j.watres.2013.03.007>
- Mi H, Yi L, Wu Q, Xia J, Zhang B (2021) Preparation of high-strength ceramsite from red mud, fly ash, and bentonite. *Ceram Int* 47:18218–18229. <https://doi.org/10.1016/j.ceramint.2021.03.141>
- Nelson NO, Mikkelsen RL, Hesterberg DL (2003) Struvite precipitation in anaerobic swine lagoon liquid: effect of pH and Mg:P ratio and determination of rate constant. *Bioresour Technol* 89:229–236. [https://doi.org/10.1016/s0960-8524\(03\)00076-2](https://doi.org/10.1016/s0960-8524(03)00076-2)
- Park JB, Craggs RJ, Sukias JP (2009) Removal of nitrate and phosphorus from hydroponic wastewater using a hybrid denitrification filter (HDF). *Bioresour Technol* 100:3175–3179. <https://doi.org/10.1016/j.biortech.2009.01.036>
- Peng L, Dai H, Wu Y, Peng Y, Lu X (2018) A comprehensive review of phosphorus recovery from wastewater by crystallization processes. *Chemosphere* 197:768–781. <https://doi.org/10.1016/j.chemosphere.2018.01.098>
- Ponvel KM, Kavitha D, Kim KM, Lee CH (2010) Adsorption of 2,4-dichlorophenol on metal-nitrate modified activated carbon. *Korean J Chem Eng* 26:1379–1382. <https://doi.org/10.1007/s11814-009-0217-4>
- Rabinovich A, Heckman JR, Lew B, Rouff AA (2021) Magnesium supplementation for improved struvite recovery from dairy lagoon wastewater. *J Environ Chem Eng* 9:105628. <https://doi.org/10.1016/j.jece.2021.105628>
- Rahman MM, Salleh MAM, Rashid U, Ahsan A, Hossain MM, Ra CS (2014) Production of slow release crystal fertilizer from wastewaters through struvite crystallization – a review. *Arabian J Chem* 7:139–155. <https://doi.org/10.1016/j.arabjc.2013.10.007>
- Ramasahayam SK, Guzman L, Gunawan G, Viswanathan T (2014) A comprehensive review of phosphorus removal technologies and processes. *J Macromol Sci A* 51:538–545. <https://doi.org/10.1080/10601325.2014.906271>
- Ren J, Li N, Wei H, Li A, Yang H (2020) Efficient removal of phosphorus from turbid water using chemical sedimentation by FeCl<sub>3</sub> in conjunction with a starch-based flocculant. *Water Res* 170:115361. <https://doi.org/10.1016/j.watres.2019.115361>
- Riley CM (2006) Relation of chemical properties to the bloating of clays. *J Am Ceram Soc* 34:121–128. <https://doi.org/10.1111/j.1151-2916.1951.tb11619.x>
- Sawada Y, Yamaguchi J, Sakurai O, Uematsu K, Mizutani N, Kato M (1979) Isothermal differential scanning calorimetry on an exothermic phenomenon during thermal decomposition of hydromagnesite 4MgCO<sub>3</sub>·Mg(OH)<sub>2</sub>·4H<sub>2</sub>O. *Thermochim Acta* 34:233–237. [https://doi.org/10.1016/0040-6031\(79\)87112-9](https://doi.org/10.1016/0040-6031(79)87112-9)
- Schott C, Cunha JR, van der Weijden RD, Buisman C (2022) Phosphorus recovery from pig manure: dissolution of struvite and formation of calcium phosphate granules during anaerobic digestion with calcium addition. *Chem Eng J* 437:135406. <https://doi.org/10.1016/j.cej.2022.135406>
- Shu J, Chen M, Wu H, Li B, Wang B, Li B, Liu R, Liu Z (2019) An innovative method for synergistic stabilization/solidification of Mn<sup>2+</sup>, NH<sub>4</sub><sup>+</sup>-N, PO<sub>4</sub><sup>3-</sup> and F<sup>-</sup> in electrolytic manganese residue and phosphogypsum. *J Hazard Mater* 376:212–222. <https://doi.org/10.1016/j.jhazmat.2019.05.017>
- Tan P (2016) Active phase, catalytic activity, and induction period of Fe/zeolite material in nonoxidative aromatization of methane. *J Catal* 338:21–29. <https://doi.org/10.1016/j.jcat.2016.01.027>
- Tang CC, Shao PH, Jian MP, Yu HG (2012) Research progress of phosphorus removal in enhanced coagulation. *Adv Mater Res* 518–523:1825–1830. <https://doi.org/10.4028/www.scientific.net/AMR.518-523.1825>
- Thistleton J, Berry TA, Pearce P, Parsons SA (2002) Mechanisms of chemical phosphorus removal II: iron (III) salts. *Process Saf Environ* 80:265–269. <https://doi.org/10.1205/095758202762277623>
- Wang F, Kuzuya T, Hirai S, Li J, Li T (2014) Carbon dioxide absorption and release properties of pyrolysis products of dolomite calcined in vacuum atmosphere. *Sci World J* 2014:862762. <https://doi.org/10.1155/2014/862762>
- Watanabe H, Hashimoto K, Misaizu F, Fuke K, Iwata S (1995) Molecular orbital studies of the structures and reactions of singly charged magnesium ion with water clusters, Mg<sup>+</sup>(H<sub>2</sub>O)<sub>n</sub>. *J Am Chem Soc* 117:755–763. <https://doi.org/10.1021/ja00107a019>
- Xie F, Wu F, Liu G, Mu Y, Feng C, Wang H, Giesy JP (2014) Removal of phosphate from eutrophic lakes through adsorption by in situ formation of magnesium hydroxide from diatomite. *Environ Sci Technol* 48:582–590. <https://doi.org/10.1021/es4037379>
- Xie S, Liu Y, Deng J, Yang J, Zhao X, Han Z, Zhang K, Wang Y, Arandiyana H, Dai H (2018) Mesoporous CoO-supported palladium nanocatalysts with high performance for o-xylene combustion. *Catal Sci Technol* 8:806–816. <https://doi.org/10.1039/c7cy02007d>
- Xu X, Chen Y, Zhou W, Zhong Y, Guan D, Shao Z (2018) Earth-abundant silicon for facilitating water oxidation over iron-based perovskite electrocatalyst. *Adv Mater Interfaces* 5:1701693. <https://doi.org/10.1002/admi.201701693>
- Yang K, Li Z, Zhang H, Qian J, Chen G (2010) Municipal wastewater phosphorus removal by coagulation. *Environ Technol* 31:601–609. <https://doi.org/10.1080/09593330903573223>
- Yang R, Zhu J, Li Y, Zhang H (2016) A study on the preparation of regular multiple micro-electrolysis filler and the application in

- pretreatment of oil refinery wastewater. *Int J Env Res Pub He* 13:457–471. <https://doi.org/10.3390/ijerph13050457>
- Yang Z, Ma Y, Liu Y, Li Q, Zhou Z, Ren Z (2017) Degradation of organic pollutants in near-neutral pH solution by Fe-C micro-electrolysis system. *Chem Eng J* 315:403–414. <https://doi.org/10.1016/j.cej.2017.01.042>
- Yang S, Sun H, Su S, Han G, Huang Y (2021) Fabrication, characterizations and performance of a high-efficiency micro-electrolysis filler for isobutyl xanthate (IBX) degradation. *J Hazard Mater* 403:123640. <https://doi.org/10.1016/j.jhazmat.2020.123640>
- Yin H, Kong M (2014) Simultaneous removal of ammonium and phosphate from eutrophic waters using natural calcium-rich attapulgite-based versatile adsorbent. *Desalination* 351:128–137. <https://doi.org/10.1016/j.desal.2014.07.029>
- Zhang T, Ding L, Ren H (2009) Pretreatment of ammonium removal from landfill leachate by chemical precipitation. *J Hazard Mater* 166:911–915. <https://doi.org/10.1016/j.jhazmat.2008.11.101>
- Zhang L, Yue Q, Yang K, Zhao P, Gao B (2018) Enhanced phosphorus and ciprofloxacin removal in a modified BAF system by configuring Fe-C micro electrolysis: investigation on pollutants removal and degradation mechanisms. *J Hazard Mater* 342:705–714. <https://doi.org/10.1016/j.jhazmat.2017.09.010>
- Zhang M, Yang J, Wang H, Lv Q, Xue J (2021) Enhanced removal of phosphate from aqueous solution using Mg/Fe modified biochar derived from excess activated sludge: removal mechanism and environmental risk. *Environ Sci Pollut Res Int* 28:16282–16297. <https://doi.org/10.1007/s11356-020-12180-2>
- Zhang L, Wang Y, Hao S, Dou Q, Lan S, Peng Y (2022) Anammox-synchronous zero-valent iron oxidation promoting synergistic nitrogen and phosphorus removal from wastewater. *Bioresour Technol* 347:126365. <https://doi.org/10.1016/j.biortech.2021.126365>
- Zhao J, Gao J, Liu J (2020) Preparation of a new iron-carbon-loaded constructed wetland substrate and enhanced phosphorus removal performance. *Materials* 13:4739. <https://doi.org/10.3390/ma13214739>
- Zhao W, Bi X, Peng Y, Bai M (2022) Research advances of the phosphorus-accumulating organisms of *Candidatus Accumulibacter*, *Dechloromonas* and *Tetrasphaera*: metabolic mechanisms, applications and influencing factors. *Chemosphere* 307:135675. <https://doi.org/10.1016/j.chemosphere.2022.135675>
- Zhou Z, Qiao W, Lin Y, Shen X, Hu D, Zhang J, Jiang LM, Wang L (2014) Phosphonate removal from discharged circulating cooling water using iron-carbon micro-electrolysis. *Water Sci Technol* 70:524–532. <https://doi.org/10.2166/wst.2014.248>
- Zhou J, Liu P, Liu Z, Zhang J, Huang X (2020) Simultaneous recovery of phosphorus with nickel purification in nickel-plating wastewater via Fe/C activated H<sub>2</sub>O<sub>2</sub> oxidation. *Chem Eng J* 381:122702. <https://doi.org/10.1016/j.cej.2019.122702>
- Zhu Q, Xing Z (2018) Simultaneous removal of nitrogen and phosphorus by magnesium-modified calcium silicate core-shell material in water. *Ecotox Environ Safe* 163:656–664. <https://doi.org/10.1016/j.ecoenv.2018.07.120>
- Zhu S, Gao J, Ba K (2014) Removal of phosphorus from domestic sewage by iron-carbon micro-electrolysis under dynamic and continuous conditions. *Fresen Environ Bull* 23:1006–1011
- Zhu D, Chen Y, Yang H, Wang S, Wang X, Zhang S, Chen H (2020) Synthesis and characterization of magnesium oxide nanoparticle-containing biochar composites for efficient phosphorus removal from aqueous solution. *Chemosphere* 247:125847. <https://doi.org/10.1016/j.chemosphere.2020.125847>
- Zou H, Wang Y (2016) Phosphorus removal and recovery from domestic wastewater in a novel process of enhanced biological phosphorus removal coupled with crystallization. *Bioresour Technol* 211:87–92. <https://doi.org/10.1016/j.biortech.2016.03.073>

**Publisher's note** Springer Nature remains neutral with regard to jurisdictional claims in published maps and institutional affiliations.

Springer Nature or its licensor holds exclusive rights to this article under a publishing agreement with the author(s) or other rightsholder(s); author self-archiving of the accepted manuscript version of this article is solely governed by the terms of such publishing agreement and applicable law.